INTERNATIONAL ATOMIC ENERGY AGENCY
UNITED NATIONS EDUCATIONAL, SCIENTIFIC AND CULTURAL ORGANIZATION
INTERNATIONAL CENTRE FOR THEORETICAL PHYSICS
I.C.T.P., P.O. BOX 586, 34100 TRIESTE, ITALY, CABLE: CENTRATOM TRIESTE

SMR. 758 - 33

SPRING COLLEGE IN CONDENSED MATTER ON QUANTUM PHASES

(3 May - 10 June 1994)

==========

REPRINTS ON THE MOTT TRANSITION IN INFINITE DIMENSIONS

Antoine GEORGES
Laboratoire de Physique
L'Ecole Normale Superieure
24 Rue Lhomond
F-75231 Paris Cedex, France

and

Gabriel KOTLIAR
Serin Physics Laboratory
Rutgers University
Piscataway, NJ 08854
U.S.A.

==========

These are preliminary lecture notes, intended only for distribution to participants.

==========

Physical properties of the half-filled Hubbard model in infinite dimensions

Antoine Georges*
Laboratoire de Physique Théorique de l'Ecole Normale Supérieure, 24, rue Lhomond, 75231 Paris Cedex 05, France

Werner Krauth†
Laboratoire de Physique Statistique de l'Ecole Normale Supérieure, 24, rue Lhomond, 75231 Paris Cedex 05, France

(Received 14 September 1992; revised manuscript received 11 February 1993)

A detailed quantitative study of the physical properties of the infinite-dimensional Hubbard model at half filling is presented. The method makes use of an exact mapping onto a single-impurity model supplemented by a self-consistency condition. This coupled problem is solved numerically. Results for thermodynamic quantities (specific heat, entropy,...), one-particle spectral properties, and magnetic properties (response to a uniform magnetic field) are presented and discussed. The nature of the Mott-Hubbard metal-insulator transition found in this model is investigated. A numerical solution of the mean-field equations *inside* the antiferromagnetic phase is also reported.

I. INTRODUCTION

Strongly correlated fermion systems have been the subject of a considerable amount of work in the last few years. The cuprate superconductors and heavy-fermion materials provide outstanding physical motivation, but along the way many aspects of "older" physical systems, such as liquid ^{3}He or Mott insulators, are being discussed anew.

The difficulty of these problems is not to be found only in the absence of any obvious small parameter in the strong-coupling regime. More deeply, it is due to the difficulty of handling simultaneously *itinerant aspects* (spatial correlations) and *atomic aspects* (on-site quantum fluctuations) in a single theoretical scheme. It is the interplay of these two characters which is at the heart of the problem, especially for the regime of intermediate couplings relevant to many of the above examples.

Recently, significant advances have been made in understanding strongly correlated fermion models in the limit of *infinite spatial dimensionality* ($d \to \infty$) first investigated by Metzner and Vollhardt.[1,2] This limit has been shown[3-5] to provide a natural generalization to quantum many-body problems of the *mean-field theory*, familiar in statistical mechanics. Most importantly, it deals with itinerant and atomic aspects on an equal footing and captures their interplay. Exact "mean-field" equations for the Green's functions have been established in this limit,[6,7,3,4] which map the problem onto a *single-impurity* quantum problem supplemented by a *self-consistency* condition.[3,4] This makes the problem amenable to various analytical and numerical treatments. Most recently, three independent works have demonstrated the possibility of a full numerical solution of the $d = \infty$ Hubbard model using this mapping.[8-10]

The aim of this paper is to give a detailed and quantitative discussion of the $d = \infty$ Hubbard model at half filling, putting the emphasis on the calculation of *physical quantities* (e.g., thermodynamics, excitation spectrum,...). We use two complementary methods. The first is the (essentially exact) numerical technique of Ref. 9 that we use for the computation of imaginary-time Green's functions, thermodynamic quantities, and in order to study the response to external fields at finite temperature. The second (approximate) method is based on the iteration of a weak-coupling scheme. It was first introduced in Ref. 3 and recently elaborated upon in Ref. 11. It can be used directly at zero temperature and yields real-frequency dynamic quantities and spectral densities. The two methods are found to agree with each other in a spectacular way in phases with unbroken spin and translational symmetry, as previously observed in Ref. 11.

Besides calculating physical quantities in the paramagnetic phase of the model, we also demonstrate in this paper that the $d = \infty$ mean-field equations can be solved numerically in the antiferromagnetic phase and in the presence of an external magnetic field. The first numerical calculation of uniform and staggered magnetizations is presented using this method.

This paper is organized as follows. In Sec. II, we define the model and establish notations (Sec. II A), summarize the equations for the single-particle Green's functions with emphasis on their mean-field content (Sec. II B), and review the connection with the Anderson-Wolff model of a magnetic impurity (Sec. II C). Section III is devoted to the explanation of the methods of the solution: full numerical solution (Sec. III A) and approximation scheme based on "iterated perturbation theory" (Sec. III B). To facilitate the reading of this paper, an overview of the phase diagram and phase transitions found subsequently is given in Sec. IV. We find two equilibrium phases: a two-sublattice antiferromagnet at low temperatures, also studied in Ref. 8, and a paramagnetic phase. In addition, as reported in Refs. 9 and 10, the paramagnetic equations display an instability, which corresponds to a transition between a *paramagnetic metal* (Fermi liquid) for weak coupling and a *paramagnetic Mott-Hubbard insulator* for strong coupling.

The rest of the paper is devoted to a detailed presenta-

0163-1829/93/48(10)/7167(16)/$06.00

tion of the physical properties of each of these regimes: the paramagnetic itinerant regime in Sec. V, the Mott-Hubbard localized paramagnet in Sec. VI, and the antiferromagnetic phase in Sec. VII.

II. EXACT MEAN-FIELD PICTURE IN $D \to \infty$

A. Model and notations

We consider in this paper the Hubbard model[12]

$$H = \sum_{\langle ij \rangle \sigma} t_{ij} c_{i\sigma}^{\dagger} c_{j\sigma} + \text{H.c.} + U \sum_{i} n_{i\uparrow} n_{i\downarrow} \tag{1}$$

with nearest-neighbor hopping on a lattice of connectivity z. Two specific cases will be considered: the d-dimensional hypercubic (hc) lattice ($z = 2d$) and the Bethe lattice (Cayley tree), both in the limit $z \to \infty$. In order for the kinetic and interaction energies to remain of the same order of magnitude in this limit, the hopping must be scaled[1] as $t_{ij} = t_* / \sqrt{2z}$. The free ($U = 0$) density of states (DOS) $D(\epsilon) = \sum_{\mathbf{k}} \delta(\epsilon - \epsilon_{\mathbf{k}})$ then acquires the following limit forms:[1,2]

Hypercubic lattice, $d \to \infty$: $$D(\epsilon) = \frac{1}{t_* \sqrt{\pi}} e^{-(\epsilon/t_*)^2} , \tag{2}$$

Bethe lattice, $z \to \infty$: $$D(\epsilon) = \frac{1}{\pi t_*} \sqrt{2 - (\epsilon/t_*)^2} . \tag{3}$$

Unless explicitly stated, we will everywhere set $t_* = 1$ in the following. As a simple consequence of the central limit theorem, a Gaussian distribution is obtained on the hypercubic lattice. It is unbounded because of "exceptional" values of the momentum (such as $\mathbf{k} = 0$) for which $\epsilon_{\mathbf{k}} = O(d)$. Some details of the physics depend on this feature. Note, however, that both distributions have a *finite* kinetic energy per particle ϵ_0, and in this sense a finite bandwidth [at half filling $\epsilon_0 = -t_* / \sqrt{\pi}$, $-4\sqrt{2} t_* / 3\pi$ for (2) and (3) respectively].

It is also important to notice that the $1/\sqrt{z}$ scaling leads to an antiferromagnetic exchange coupling $J_{ij} \sim t_{ij}^2 / U = O(1/z)$ which is precisely such that *finite* transition temperatures (and hence, ordered phases) are kept in the $z \to \infty$ limit. Indeed the exchange energy between one site and its shell of z neighbors with opposite spins remains $O(1)$. The fact that the *individual* exchange between two given spins vanishes as $z \to \infty$ has some important physical consequences however (see, e.g., Sec. VI C).

B. Mean-field equations

We deal extensively in this paper with the single-particle Green's function, defined at finite temperature by

$$G_{ij,\sigma}(\tau - \tau') = -\langle T c_{i,\sigma}(\tau) c_{j,\sigma}^{\dagger}(\tau') \rangle ,$$

where the imaginary time τ runs between 0 and $\beta = 1/T$. Let us consider first a phase with unbroken spin and translation invariance, and define the self-energy in the usual way [$\omega_n = (2n+1)\pi/\beta$]:

$$G(\mathbf{k}, i\omega_n) = \frac{1}{i\omega_n + \mu - \epsilon_{\mathbf{k}} - \Sigma} . \tag{4}$$

In the limit $z = \infty$, the self-energy no longer depends on momentum: $\Sigma = \Sigma(i\omega_n)$.[13] Hence, all the information on single-particle properties is encoded in a function of frequency only. The underlying physical reason for this simplification is that the $z \to \infty$ limit freezes *spatial* fluctuations but retains the nontrivial dynamics of *temporal* on-site fluctuations between the four possible states: $|0\rangle$, $|\uparrow\rangle$, $|\downarrow\rangle$, and $|\uparrow,\downarrow\rangle$. As recently realized in several works,[7,6,3,4] it is thus possible to obtain all single-particle properties from the study of a *single-site* problem which describes the effective dynamics of these fluctuations. We follow here the formulation of Refs. 3 and 4, in which the effective action for this single-site problem is shown to be

$$\mathcal{S} = U \int_0^{\beta} d\tau\, n_{\uparrow}(\tau) n_{\downarrow}(\tau) - \int_0^{\beta} d\tau \int_0^{\beta} d\tau' \sum_{\sigma} c_{\sigma}^{\dagger}(\tau) [(\partial_{\tau} + \mu)\delta(\tau - \tau') - \mathcal{A}(\tau - \tau')] c_{\sigma}(\tau') . \tag{5}$$

Here, $\mathcal{A}(\tau - \tau')$ is an effective two-body amplitude which describes processes in which an electron leaves the site, wanders among the rest of the lattice, and comes back (or is replaced by another with equal spin) at a later time. $\mathcal{A}(\tau - \tau')$ depends on the processes happening on all the other sites and hence is *not known explicitly*. It is related to the interacting Green's function of $\mathcal{S}$, $G(\tau - \tau') = \langle T c(\tau) c^{\dagger}(\tau') \rangle_{\mathcal{S}}$, by a self-consistency condition which reads

$$G(i\omega_n) = D[i\omega_n + \mu - \mathcal{A}(i\omega_n) - G(i\omega_n)^{-1}] . \tag{6}$$

In this expression, D denotes the Hilbert transform of $D(\epsilon)$: $\tilde{D}(z) = \int d\epsilon D(\epsilon)/(z - \epsilon)$. A solution of the single-site problem (5) supplemented by the constraint (6) fully determines $G(i\omega_n)$ and $\mathcal{A}(i\omega_n)$ in a coupled manner. The self-energy Σ is related to this solution by

$$i\omega_n + \mu - \Sigma(i\omega_n) = \mathcal{A}(i\omega_n) + G(i\omega_n)^{-1} . \tag{7}$$

This identification is such that $G(i\omega_n)$ just coincides with the *site-diagonal* Green's function of the lattice model: $G(i\omega_n) = \sum_{\mathbf{k}} G(\mathbf{k}, i\omega_n)$, as expressed by (6). The notations used here are slightly different from those of our previous papers,[3,4,9] in which we denoted by G_0 the function which plays the role of the "bare" Green's function in the single-site action $\mathcal{S}$:

$$G_0(i\omega_n)^{-1} = i\omega_n + \mu - \mathcal{A}(i\omega_n) . \tag{8}$$

Whenever convenient, we shall make use of this alterna-

tive notation below [G_0 is *not to be confused* with the free ($U=0$) on-site Green's function however].

Equations (5) and (6) are *exact* for the hypercubic and Bethe lattices in the limit $z \to \infty$.[14] They have the physical content of a *mean-field theory* in which a lattice problem is reduced to a single-site problem whose dynamics is self-consistently related to the rest of the lattice which plays the role of an "external bath" for the isolated site.

Explicit expressions can be given for the Hilbert transform $\tilde{D}$ for both the Gaussian and semicircular DOS. They read

$$\tilde{D}(\zeta) = -is\sqrt{\pi}\exp(-\zeta^2)\operatorname{erfc}(-is\zeta)$$

with $s=\operatorname{sgn}(\operatorname{Im}\zeta)$ in the former and $\tilde{D}(\zeta)=\zeta-\sqrt{\zeta^2-2}$ in the latter ($t_*=1$).[15] This last expression allows one to rewrite the self-consistency condition (6) for the Bethe lattice in a much simpler form:

$$\text{Bethe lattice: } \mathcal{A}(i\omega_n)=\frac{t_*^2}{2}G(i\omega_n)\ . \tag{9}$$

Due to the absence of loops in this case, the effective on-site amplitude just coincides with the on-site Green's function itself.

It is instructive to check these equations in two simple limits. In the free limit $U=0$, (5) is solved by $G^{-1}=i\omega_n+\mu-\mathcal{A}$, and hence from (6), $G(i\omega_n)=\tilde{D}(i\omega_n+\mu)$ reduces to the free on-site Green's function ($\Sigma=0$). In the "atomic" limit $t_*=0$, one just has a collection of disconnected sites and $D(\epsilon)$ becomes a δ function, with $\tilde{D}(\zeta)=1/\zeta$. Then (6) implies $\mathcal{A}(i\omega_n)=0$ and the effective action $\mathcal{S}$ becomes essentially local in time and describes a four-state Hamiltonian which yields

$$G(i\omega_n)_{\text{at}}=(1-n/2)/(i\omega_n+\mu)+n/2(i\omega_n+\mu-U)\ ,$$

with

$$n/2=(e^{\beta\mu}+e^{\beta(2\mu-U)})/(1+2e^{\beta\mu}+e^{\beta(2\mu-U)})\ .$$

The above equations are valid in the absence of any spin or translational symmetry breaking. In the following, however, we shall need a generalization of these equations[1,7] to the following cases.

(i) Uniform applied field $h\sum_i(n_{i\uparrow}-n_{i\downarrow})$. The above equations are then trivially extended by separating the two spin species, allowing for two different amplitudes $\mathcal{A}_\uparrow, \mathcal{A}_\downarrow$ in $\mathcal{S}$, replacing $\mathcal{A}$ everywhere by the corresponding $\mathcal{A}_\sigma$ and μ by $\mu+h\sigma$. In particular, the self-consistency relation does not mix spin species, and reads

$$G_\sigma=\tilde{D}(\mathcal{A}_\sigma+G_\sigma^{-1})\ . \tag{10}$$

(ii) Antiferromagnetic phase with two-sublattice long-range order. Again, one has to allow for two separate amplitudes $\mathcal{A}_\uparrow, \mathcal{A}_\downarrow$ in $\mathcal{S}$, but the self-consistency condition now mixes both spin species, and reads (on, e.g., sublattice A)

$$G_{A\sigma}=\sqrt{\zeta_{B\sigma}/\zeta_{A\sigma}}\,\tilde{D}(\sqrt{\zeta_{A\sigma}\zeta_{B\sigma}}) \tag{11}$$

with $\zeta_{A\sigma}=\mathcal{A}_{A\sigma}+G_{A\sigma}^{-1}=i\omega_n+\mu-\Sigma_{A\sigma}$. The self-energy is still purely site diagonal, but depends on the sublattice, with $\Sigma_{A\uparrow}=\Sigma_{B\downarrow}(\simeq\Sigma_\uparrow)$ and $\Sigma_{B\uparrow}=\Sigma_{A\downarrow}(\simeq\Sigma_\downarrow)$.

One is also interested in computing *response functions* (e.g., spin and charge susceptibilities) of the lattice model. It is possible to reduce this calculation to a set of linear equations involving vertex functions of the *impurity problem*.[16,8] This has been successfully used in actual computations.[8] In the following, however, we use an alternative method, which is to solve the above equations for the *single-particle* Green's functions in the presence of a finite external "field" (e.g., h or μ), and to deduce the response function from the small field behavior. This method avoids the calculation of vertex functions and provides information on the finite-field behavior, which is of great physical interest in itself, especially for the response to a uniform magnetic field (Sec. V D).

Thermodynamic properties can also be obtained from impurity-model quantities. The single-particle Green's function directly yields the internal energy[17]

$$\frac{E}{N}=T\sum_{n,\sigma}\int_{-\infty}^{+\infty}d\epsilon\frac{\epsilon D(\epsilon)}{i\omega_n+\mu+h\sigma-\Sigma_\sigma(i\omega_n)-\epsilon}$$
$$+\tfrac{1}{2}T\sum_{n,\sigma}\Sigma_\sigma(i\omega_n)G_\sigma(i\omega_n) \tag{12}$$

while the grand-canonical free energy of the lattice model is related to the impurity model free energy by[7,4]

$$\frac{\Omega}{N}=\Omega_{\text{imp}}-T\sum_{n,\sigma}e^{i\omega_n 0^+}\left[\int_{-\infty}^{+\infty}d\epsilon\,D(\epsilon)\ln[i\omega_n+\mu+h\sigma-\Sigma_\sigma(i\omega_n)-\epsilon]+\ln G_\sigma(i\omega_n)\right]\ . \tag{13}$$

This paper deals with the properties of the half-filled case, $\langle n_\uparrow\rangle+\langle n_\downarrow\rangle=1$. Then, particle-hole symmetry implies that $\mu=U/2$, and it is useful to define "shifted" quantities by

$$\hat{G}_0^{-1}=G_0^{-1}-U/2,\quad \hat{\Sigma}=\Sigma-U/2\ . \tag{14}$$

In addition to the standard fermionic symmetry, $G_\sigma(\tau+\beta)=-G_\sigma(\tau)$, the following symmetry properties then hold:

$$F_\sigma(-i\omega_n)=-F_{-\sigma}(i\omega_n)$$
$$\Leftrightarrow F_\sigma(\beta-\tau)=-F_{-\sigma}(\tau)(\text{half filling})\ , \tag{15}$$

where F stands for any of the functions $G, \mathcal{A}, \hat{\Sigma}$, and $\hat{G}_0$. In particular, note that

$$G_\sigma(\tau=0^-)=\langle n_\sigma\rangle=1-\langle n_{-\sigma}\rangle=1+G_\sigma(\tau=0^+)\ .$$

C. Connection with single-impurity models

As pointed out in Refs. 3 and 4, the single-site action (5) can be thought of as describing a magnetic impurity coupled to a bath of conduction electrons. In this picture, the single site plays the role of the impurity orbital, while the role of the bath is played by the rest of the lattice, which generates $\mathcal{A}(\tau-\tau')$. The hybridization is via the hopping t_*. This point of view can be made precise by introducing the following spectral representation:

$$\mathcal{A}(i\omega_n)=\int_{-\infty}^{+\infty}\frac{\Delta(\omega)}{i\omega_n-\omega}\,d\omega\ . \tag{16}$$

With this parametrization, the action $\mathcal{S}$ exactly coincides with the effective action for the d orbital in the Anderson model,[18] once the conduction electrons have been integrated out. To see this, let us consider the Anderson model (in the particle-hole symmetric case, corresponding to half-filling, for simplicity):

$$H_{\mathrm{AM}}=\sum_{k\sigma}\omega_k a^{\dagger}_{k\sigma}a_{k\sigma}+U(n_{d\uparrow}-\tfrac{1}{2})(n_{d\downarrow}-\tfrac{1}{2})+\sum_{k\sigma}\left[V_k a^{\dagger}_{k\sigma}d_{\sigma}+\mathrm{H.c.}\right]. \tag{17}$$

Performing the Gaussian integral over the $a_{k\sigma}$'s, the effective action for the d level is found to coincide with $\mathcal{S}$ with the identifications $\mu=U/2$ and $\Delta(\omega)_{\mathrm{AM}}=\sum_k|V_k|^2\delta(\omega-\omega_k)$. Hence the spectral density $\Delta(\omega)$ associated with $\mathcal{A}(i\omega_n)$ can be thought of as the density of states defining the conduction electron "bath" in the Anderson model picture. This is even more clear in the case of the Bethe lattice: there, one can identify $V_k=t_*/\sqrt{2}$ as the effective hybridization and the self-consistency can be written as $\Delta(\omega)=(t_*/\sqrt{2})^2\rho(\omega)$, which means that the density of states of the bath coincides with the one-particle local spectral density $\rho(\omega)=-1/\pi\,\mathrm{Im}G(\omega+i0^+)$.

Equivalently, one could view the single-site action as a Wolff model [i.e., an electron gas with DOS $\rho(\omega)$ in which U acts only on a single site[19]].

III. METHODS OF SOLUTION

A calculation of the one-particle properties of the $d=\infty$ Hubbard model requires a solution of the *coupled* problem defined by Eqs. (5) and (6). The amplitude $\mathcal{A}(i\omega_n)$ (or alternatively, the "bare" Green's function of $\mathcal{S}$: $G_0(i\omega_n)^{-1}=[i\omega_n+\mu-\mathcal{A}(i\omega_n)]^{-1}$) is not explicitly known from the start. Hence, we use a method based on the iteration of the two following steps: (i) the calculation of the impurity Green's function G for a given G_0 (ii) the calculation of an updated function $G_{0,\mathrm{new}}$ from the above solution. This is achieved by first Fourier transforming[20] G_0 and G and then using the self-consistent equation (6) in the form

$$G_{0,\mathrm{new}}(i\omega_n)^{-1}=\Sigma(i\omega_n)+1/\bar{D}[i\omega_n+\mu-\Sigma(i\omega_n)]\ ,$$

where $\Sigma(i\omega_n)=G_0(i\omega_n)^{-1}-G(i\omega_n)^{-1}$.

This procedure is iterated at a fixed value of the chemical potential μ until convergence is reached, starting from an arbitrary G_0.

The difficult step of this procedure is (i), which involves solving the impurity model $\mathcal{S}$ for an essentially arbitrary G_0.[21] This is a nonlinear problem, which is also nonlocal in time, and a full solution can only be numerical.[8-10] Alternatively, one can resort to approximations to make the problem tractable. In the next subsections, we describe two methods based on these two possible strategies.

A. Numerical solution: Monte Carlo and exact enumeration methods

Since $\mathcal{S}$ can be viewed as an Anderson model, we can use the algorithm of Hirsch and Fye[22] in order to perform step (i). This algorithm works directly in terms of the imaginary-time Green's functions $G_0(\tau)$ and $G(\tau)$. The interval $[0,\beta]$ is discretized in L slices of size $\Delta\tau$, $\tau_l=l\Delta\tau$, $l=0,\ldots,L-1$ ($\beta=L\Delta\tau$). After the usual Trotter breakup, the interaction term in $\mathcal{S}$ is decoupled through L auxiliary Ising variables $\sigma(\tau_l)$:

$$e^{-\Delta\tau U n_{\uparrow}n_{\downarrow}}=\tfrac{1}{2}\mathrm{Tr}\sigma e^{\lambda\sigma(\tau_l)(n_{\uparrow}-n_{\downarrow})-U\Delta\tau(n_{\uparrow}+n_{\downarrow})/2} \tag{18}$$

with $\cosh\lambda=\exp\Delta\tau U/2$. For a given spin configuration, the trace over fermions can be taken. The computation of $G(\tau_l)$ amounts to finding the inverse of the L^*L matrix

$$O(\tau_l,\tau_l')=\hat{G}_0^{-1}(\tau_l-\tau_l')+\lambda\sigma(\tau_l)\delta_{\tau_l,\tau_l'}$$

for each of the 2^L spin configurations and to summing over configurations with a statistical weight given by the determinant of the matrix O:[23] $G(\tau-\tau')=\langle O^{-1}(\tau,\tau')\rangle_{\text{spin conf}}$. Following Hirsch and Fye,[22] this can be done most conveniently by sampling the Ising configuration space through single spin flips, and making use of Dyson's equations instead of computing explicitly the inverse of O. This reduces the number of operations from L^3 to L^2 per accepted move.

For large grids ($L\geq 18$) we have used a single-spin-flip Monte Carlo method to sample spin configurations, as in Ref. 22. For $L\leq 16$, we have been able to sum over *all* 2^L spin configurations using Gray's code,[24] which enumerates all configurations through single spin flips. This enumeration method is free of statistical noise, and can thus be considered as an *exact numerical solution* of the problem for a given discretization. Even though it is limited in grid size L, it has several advantages over the Monte Carlo method.

(1) It allows a direct calculation of the energy and free energy, using Eqs. (12) and (13).

(2) It is better suited for analytic continuations of imaginary-time data using simple Pade transform methods (rather than maximal entropy ones) (Ref. 25).

(3) It allows a precise assessment of convergence properties.

Remarkably, this iterative algorithm is found to converge rapidly to a solution (G_0,G) of Eqs. (5) and (6). Typical examples are displayed in Fig. 1 for $U=2.5$ and 5 at $\beta=10$. The results displayed are obtained by the Monte Carlo method with $L=32$, for which a conver-

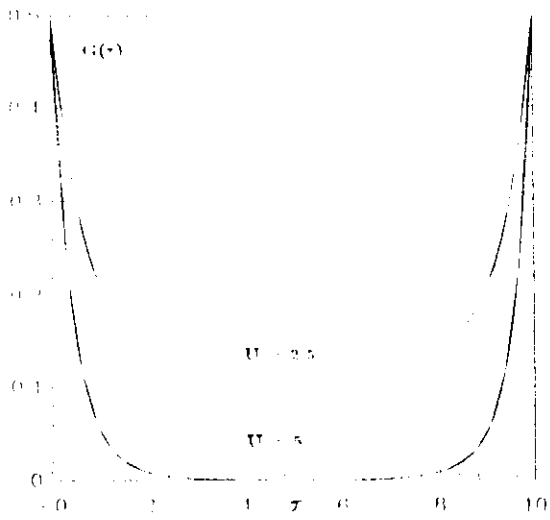

FIG. 1. The hypercubic lattice local Green's function $-G(\tau)$ vs τ at $\beta=10$, for $U/t_*=2.5$ (upper group of curves) and $U/t_*=5$ (lower group). Within each group, the lower curve is the Monte Carlo solution with $L=32$, and the upper one is the result of the iterated perturbation theory (IPT) approximate method.

gence up to 10^{-3} is obtained in four iterations with 10 000 sweeps. For the same number of iterations, an accuracy of 10^{-5} is reached when using Gray's code with $L=16$ (3 min per iteration on a HP 730 workstation).[26]

B. Iterated perturbation theory

Powerful as it is, the above numerical method is still limited by the two intrinsic weaknesses of the algorithm used: studying low temperatures requires a rapidly increasing numerical effort, and, more importantly, the algorithm produces imaginary-time quantities which do not directly yield the dynamical properties of the system (an analytic continuation is required). Hence, an approximate method which is able to deal directly with zero temperature and real frequencies is of interest. For the single-impurity problem, the interaction term $Un_\uparrow n_\downarrow$ is known to be a fairly regular perturbation, and much useful qualitative and quantitative information on the Anderson model has been obtained in the past using weak-coupling approaches.[27]

Motivated by this remark, a method was introduced in Ref. 3, which is again based on the iteration of steps (i) and (ii), but simply makes use of a weak-coupling calculation to second order in U in order to compute the self-energy Σ (and hence G) from G_0 in step (i). We call this method the iterated perturbation theory (IPT). Obviously, it can be easily performed at any finite temperature, or directly at zero temperature using real-frequency Green's functions

$$G(\omega)=\theta(\omega)G(\omega+i0^+)+\theta(-\omega)G(\omega-i0^+) .$$

The relevant formulas read (at half filling)

$$\hat{\Sigma}_n(i\omega_n)=U^2\int_0^\beta d\tau\, e^{i\omega_n\tau}\hat{G}_{0,-\sigma}(\tau)^3 , \tag{19}$$

$$T=0:\ \hat{\Sigma}_n(\omega)=-U^2\int_{-\infty}^{+\infty} dt\, e^{i\omega t}\hat{G}_{0,-\sigma}(t)^3 . \tag{20}$$

Various alternative methods based on weak-coupling have been used by other authors in the present context of the $d=\infty$ lattice model, namely, plain weak-coupling perturbation theory to $O(U^2)$ in which the *free* local Green's function $\tilde{D}(i\omega_n)$ is used in (19) and (20) in place of $\hat{G}_0$,[28] and self-consistent weak-coupling approaches[29] which attempt to find a solution with the *interacting* G replacing $\hat{G}_0$ in (19) and (20). This has also been generalized to include bubble and ladder summations in Ref. 30.

All three methods, of course, coincide for very small values of U. It has been noticed, however,[3] that the results of the self-consistent perturbation theory are in *qualitative disagreement* with both plain weak coupling and IPT already for moderate values of U: only the latter method accounts correctly for the high-energy properties of the excitation spectrum, and, in particular, for the formation of the upper Hubbard band.

Recently, insightful remarks by Zhang *et al.* have put the IPT method on a much firmer basis.[11] They noticed that, remarkably, IPT yields the *exact result* in the *atomic limit* $t_*=0$ at half filling. Indeed, the self-consistency equation (6) implies that $\hat{G}_0=1/i\omega_n$ in this limit, for which formulas (19) and (20) lead to $\hat{\Sigma}=U^2/4i\omega_n$, the exact atomic answer. From this remark, one can expect IPT to provide a satisfactory *interpolation between the small- and large-U limits.* Indeed, as first noticed in Ref. 11, a coupled solution of the IPT equations can be found at *arbitrary large values of U* and is found to be in remarkable agreement with the corresponding numerical results down to the lowest temperatures where the latter can be obtained. A direct comparison is made in Fig. 1 for $U=2.5$ and 5 at $\beta=10$. It will be shown below that the paramagnetic solution has a phase transition for a finite $U=U_c$ at $T=0$, which is quite correctly described within IPT, a feature obviously not found within a plain weak-coupling expansion.

IV. PHASE DIAGRAM AND PHASE TRANSITIONS

To make the reading of this paper easier, we give at this stage an overview of the phase diagram found at half filling using the above methods. Figure 2 displays the phase diagram for the hypercubic lattice as a function of temperature T and strength of the interaction U. Very similar results are found for the Bethe lattice. The *equilibrium* phases of the Hubbard model on both lattices are the following.

(i) An antiferromagnetic (AF) phase for $T<T_N(U)$. This phase is found by solving the mean-field equations taking into account two-sublattice long-range order, as described above. Iteration of these equations is found to converge to a broken symmetry solution with a nonzero staggered magnetization m_s for $T<T_N$, and to an unbroken solution above T_N. That the ground state is always antiferromagnetic for arbitrary U is to be expected from the bipartite character of both lattices [with $D(0)>0$].

(ii) A paramagnetic phase for $T>T_N(U)$. Another critical line $U=U_c(T)$ is indicated in Fig. 2, which corresponds to a phase transition found within the IPT

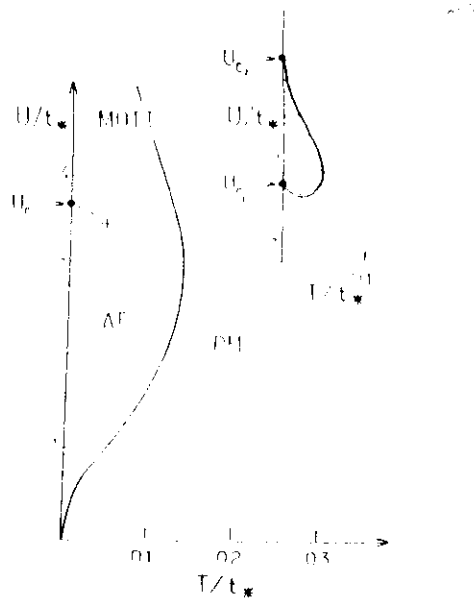

FIG. 2. Phase diagram for the hypercubic lattice. The plain line is the Néel temperature below which the antiferromagnetic (AF) phase is found. Within the IPT method, a (dashed) line of first-order transition is found between a paramagnetic metal (PM) and a Mott paramagnetic insulator (MOTT). Inset: Region of *coexistence* of a metallic and an insulating solution of the mean-field equations, as obtained in the IPT method (see also Ref. 11).

method when solving the paramagnetic form (5) and (6) of the mean-field equations, ignoring the possibility of spin-symmetry breaking. This instability has been reported previously,[9,10] and corresponds, at zero temperature, to a Mott-Hubbard transition between a paramagnetic metal for $U<U_c(T=0)\equiv U_c$ and a paramagnetic insulator for $U>U_c$. Our work and the complementary results of Ref. 11 show that $U=U_c(T)$ is a line of first-order transition (similar to a liquid-gas situation) which ends at a critical point. More precisely, we find that, close to $T=0$, an insulating solution of the paramagnetic mean-field equations can be found for $U>U_{c1}$ while, as recently reported in Ref. 11, a metallic solution exists in the whole range $U<U_{c2}$, with $U_{c2}>U_{c1}$. Hence, there is a region of the (U,T) parameter space in which *two solutions* of the equations coexist, and one has the characteristic scenario of a first-order transition. Using the IPT approximate scheme, one finds $U_c/t_*\simeq U_{c1}/t_*\simeq 3.7$ on the hc lattice ($\simeq 3.6$ on the Bethe lattice), and[11] $U_{c2}/t_*\sim 4.5$ (~ 4.7 on the Bethe lattice). The coexistence region found within IPT is displayed in the inset of Fig. 2. Note that it extends only up to temperatures of order $\sim\frac{1}{20}$. For the true (Monte Carlo) solution, the situation is somewhat unclear and deserves further numerical calculations. The nature of the Mott transition is discussed more extensively in Sec. VI E.

Let us emphasize that the metal-insulator transition at $T=0$ is not a transition occurring within the true ground state of the model (which is an antiferromagnetic insulator for all U), but only within the paramagnetic solution continued to the region where it is actually unstable towards antiferromagnetism. That such a continuation is possible (in a fully consistent way thermodynamically) will be demonstrated at length below, and is a remarkable feature of the $d=\infty$ mean-field equations. In fact, an alternative model can be found for which the paramagnetic Mott-Hubbard state is the exact ground state, without any magnetic order setting in at low temperatures.[31] It is simply defined as a Hubbard model on a *fully connected* cluster of N sites, with randomness on the hopping parameters t_{ij}:

$$H=-\sum_{\sigma;i,j=1}^{N} t_{ij}c_{i\sigma}^{\dagger}c_{j\sigma}+U\sum_i n_{i\uparrow}n_{i\downarrow}\quad \sqrt{\overline{t_{ij}^2}}=\frac{t_*}{\sqrt{2N}}\ . \tag{21}$$

It is possible to show[31] that, *in the paramagnetic phase*, the single-particle Green's function of this random model coincides with the same quantity for the Hubbard model on the $z=\infty$ Bethe lattice, with no randomness and hopping parameter $t_{ij}=t_*/\sqrt{2z}$.[32] It is clear, however, that the phase diagram of the two models differ: obviously the disordered one has a highly degenerate total singlet ground state for large U at half filling, and *no antiferromagnetic phase*. Hence, a true ground-state phase transition is found for this model between a paramagnetic Mott insulator at large U and a metal at small U. The rest of this paper is devoted to a detailed discussion of the physical properties of these various phases.

V. THE PARAMAGNETIC ITINERANT REGIME

We discuss here the physics of the paramagnetic phase below the Mott-Hubbard transition. We consider, when needed, the continuation of the paramagnetic solution down to $T=0$, ignoring in this section the occurrence of antiferromagnetism (which will be addressed in Sec. VII).

A. Energy scales and thermodynamic properties

We have computed several thermodynamic quantities as a function of temperature and U, both using the exact enumeration numerical solution and the IPT scheme at finite temperature. The basic quantity computed is the internal energy, which can be readily obtained from the imaginary-time Green's function using Eq. (12). The specific heat $C_v=d(E/N)/dT$ is then obtained by performing the simulation for two close temperatures and differentiating numerically.[33] The same calculation allows one to obtain the entropy by integration:

$$\frac{S}{N}=\ln(4)-\int_T^{+\infty}\frac{C_v(T')}{T'}dT'\ , \tag{22}$$

where we have used the high-temperature limit of ln4 (corresponding to the four possible states on each site). Note that Eq. (22) only requires knowing C_v *above* the temperature studied. Another possibility would be to compute directly the free energy from Eq. (13) but we have preferred the more economical method described here which requires only the knowledge of Green's functions.

In Fig. 3, the results obtained for C_v vs T by the

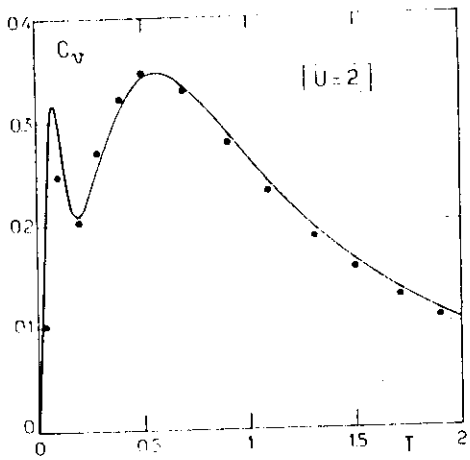

FIG. 3. Specific heat C_v vs temperature T for $U=2$ (hypercubic lattice). The points are the results of the numerical solution using exact enumeration, extrapolated to $\Delta\tau \to 0$. The solid line is obtained by the IPT method. Note that the spin and charge energy scales are already well separated.

enumeration method and the IPT scheme are displayed and compared for $U=2$. The agreement is seen to be spectacular, down to the lower temperatures studied by enumeration. This confirms for thermodynamic quantities the observation made in Ref. 11 for Green's functions. Figure 4 displays the C_v vs T curves for several values of $U < U_c$, ranging from the weak-coupling regime to the very strongly correlated metal for U close to U_c. Increasing U leads to the formation of two peaks in the specific heat, corresponding to the gradual separation of two energy scales.

(i) A low-energy scale T_F^* (or effective Fermi temperature), corresponding to the first, narrow peak in C_v vs T. As discussed below, T_F^* must be interpreted as a scale associated with local spin fluctuations and is also the scale below which a Fermi-liquid description applies. In particular, the specific heat starts linearly at low temperature, and a possible definition of T_f^* is from its slope: $C_v = T/T_f^*$ as $T \to 0$. This yields, e.g., $T_f^*(U=0) = 3/2\pi^2 D(0) \sim 0.27$ and $T_f^*(U=2) \sim 0.13$ (hypercubic lattice). T_f^* sets the scale for both the location and the width of the specific-heat peak (with this definition, T_F^* is found to lie roughly halfway between the peak maximum and the subsequent minimum). As U is increased, T_F^* decreases rapidly. The ratio $T_F^*(U)/T_F^*(0)$ is related to the effective mass and quasiparticle weight Z by (cf. Sec. V B and Fig. 8, where a plot of this ratio is given)

$$\frac{T_F^*(U)}{T_F^*(0)} = \frac{m}{m^*} = Z \ . \tag{23}$$

(ii) A high-energy scale (set by U), corresponding to the broad high-energy peak in C_v vs T. This scale is associated with on-site charge fluctuations. As U is increased, the location of this peak shifts upwards, but its width remains roughly constant, set by the bare bandwidth.

Interestingly, an intermediate range of U is found in which C_v vs T does not yet have two well-separated peaks, but rather displays a plateaulike feature (or a very shallow minimum) around T_F^*. This regime is somewhat reminiscent of the properties of liquid ^{3}He (Ref. 34) (though C_v eventually decreases in our present model because of the bounded DOS). Another puzzling feature of the results displayed in Fig. 4 is that all curves appear to cross almost at the same temperature, i.e., there apparently is a special temperature ($\simeq 0.6t_*$ for the hc lattice) at which the specific heat is independent of the strength of the interaction, to quite good accuracy. We have no simple physical explanation of this phenomena, but we note that a very similar phenomenon occurs in liquid ^{3}He,[34] if one views U as playing the role of pressure as in the quasilocalized approach.[36,35] As shown below (Fig. 15), this single crossing no longer holds in the insulating phase above U_c.

A typical result for the entropy per lattice site vs temperature is displayed in Fig. 5, for $U=2$. The overall behavior is much smoother than for C_v, but the different regimes, corresponding to the two energy scales above,

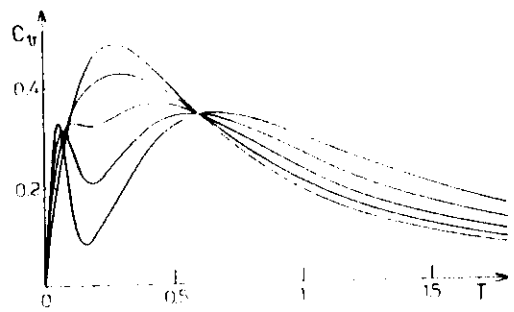

FIG. 4. Specific heat vs temperature (hc lattice) for $U=0.51$, 1, 1.5, 2, 2.5. Note the gradual increase of the linear slope with U and the gradual separation of the spin and charge scales. The curves seem to intersect at essentially the same temperature.

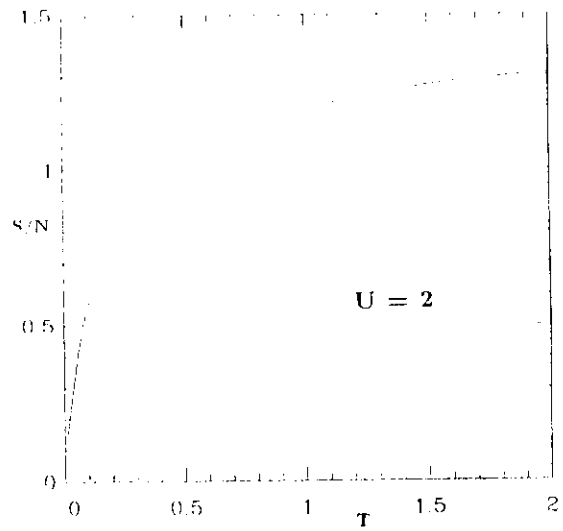

FIG. 5. Entropy per lattice site S/N vs temperature for $U=2$ (hc lattice). The value ln2 is reached roughly at the spin fluctuation scale T_F^*.

are quite clearly seen. S/N starts linearly at low temperatures, and, interestingly, reaches a value close to ln2 around $T \sim T_F^*$. This corresponds to the defreezing of the on-site spin fluctuation entropy at this scale, and is also qualitatively similar to the experimental results on ^{3}He.[34] A second regime of temperature between T_F^* and $\sim U$ corresponds to the progressive defreezing of charge fluctuations, with a slow increase of S/N from ln2 to ln4.

As a simple thermodynamic indicator of the degree of correlation of the system, we display in Fig. 6 the temperature dependence of the fraction of doubly occupied sites: $\langle D \rangle = \langle n_\uparrow n_\downarrow \rangle$, for various values of U. This is easily computed as an average over Ising spin configurations in the numerical simulation of the single-site problem (note that $\langle D \rangle$ is related to the impurity orbital local moment by $2\langle D \rangle = 1 - \langle S_z^2 \rangle$). At very high temperature ($T \gg U$), $\langle D \rangle$ becomes asymptotic to the atomic value $\langle D \rangle_{at} = 1/[2+2\exp(U/2T)]$ and tends to $\frac{1}{4}$ as expected. The data display a characteristic low-temperature behavior: for U not too large, $\langle D \rangle$ initially *decreases* with temperature, reaches a minimum for $T = T_m$, and increases again. The inset of Fig. 6 shows the dependence of T_m on U. This behavior is characteristic of incipient localization effects in a strongly correlated Fermi liquid in a regime dominated by spin fluctuations.[37] Starting from the low-temperature Fermi-liquid regime with an entropy $\simeq T/T_F^*$ per particle, the system can gain free energy when increasing temperature by increasingly localizing the particles (i.e., decreasing $\langle D \rangle$) in order to take advantage of a larger spin entropy. The same physical reason is responsible for the negative slope of the metal-insulator transition line $U_c(T)$ (Fig. 2), so that one can go from the itinerant to the localized phase upon heating. This is also observed in the phase diagram of liquid ^{3}He below the Pomeranchuk temperature and of transition-metal oxides such as V_2O_3.[38]

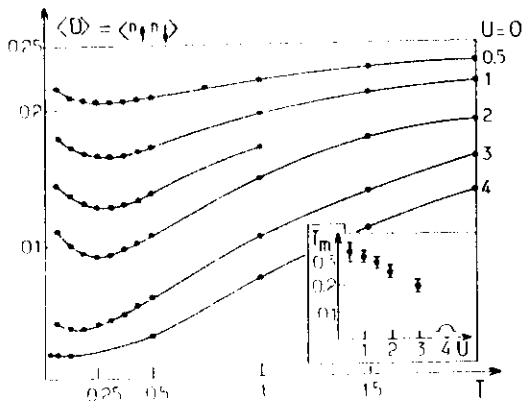

FIG. 6. Fraction of doubly occupied sites $\langle D \rangle$ vs temperature for the hc lattice with $U = 0, 0.5, 1, 2, 3, 4$ (exact enumeration and Monte Carlo results). Inset: Temperature T_m at which the minimum of $\langle D \rangle$ vs T is found, as a function of U. For $U = 4$, we cannot find a minimum down to the lowest temperature studied ($\beta = 32$).

B. Zero-temperature results and Fermi-liquid description

We now study, using the IPT method, the zero-temperature properties of the metallic solution of the paramagnetic equations, which exists[11] for $U < U_{c2}$. Typical results for the real and imaginary parts of the $T=0$ (retarded) self-energy are displayed in Fig. 7. A Fermi-liquid description of the low-frequency behavior applies, with

$$\mathrm{Re}\Sigma(\omega + i0^+) = U/2 + (1 - 1/Z)\omega + O(\omega^3) , \tag{24}$$

$$\mathrm{Im}\Sigma(\omega + i0^+) = -\gamma\omega^2 + O(\omega^4) . \tag{25}$$

The constant term $U/2$ is such that the Luttinger theorem is satisfied, with $\Sigma(i0^+) = \mu = U/2$, so that the Fermi surface is unchanged by the interactions in the metallic phase. Note that, because $\Sigma(\omega)$ is momentum independent, the Fermi surface not only retains its volume, but also its *shape*.[13] For the same reason, the quasiparticle weight Z is directly related to the effective mass by[13] $m^*/m = 1/Z$ and controls the spin-fluctuation scale introduced above [Eq. (23)]. A plot of the IPT results for Z is given in Fig. 8 for both the hypercubic and Bethe lattices. Z decreases rapidly with increasing U, and jumps discontinuously to zero at the first-order Mott transition $U_c(T=0)$ (the values of Z corresponding to the metallic solution in the range $U_c < U < U_{c2}$ are not displayed in Fig. 8). We also display in Fig. 9 the momentum distribution of particles $N(\epsilon_k)$, showing the progressive reduction of the discontinuity (of height Z) as U is increased.

The IPT method also yields information about the excitation spectrum, through the $T=0$ local one-particle spectral density:

$$\rho(\omega) = -\frac{1}{\pi}\mathrm{Im}\sum_{\mathbf{k}} G(\mathbf{k}, \omega + i0^+) . \tag{26}$$

This quantity is displayed in Fig. 10 for several values of U. As U is increased from zero, $\rho(\omega)$ develops three well-separated structures:[3] a narrow quasiparticle peak

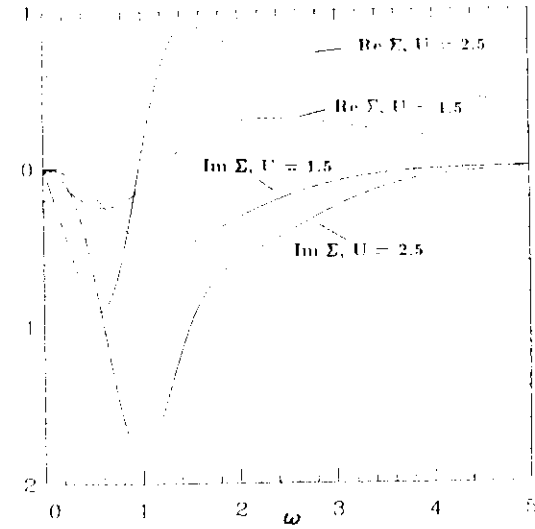

FIG. 7. $\mathrm{Re}\Sigma(\omega + i0^+)$ and $\mathrm{Im}\Sigma(\omega + i0^+)$ at $U = 1.5$ and 2.5 (hc lattice, IPT method).

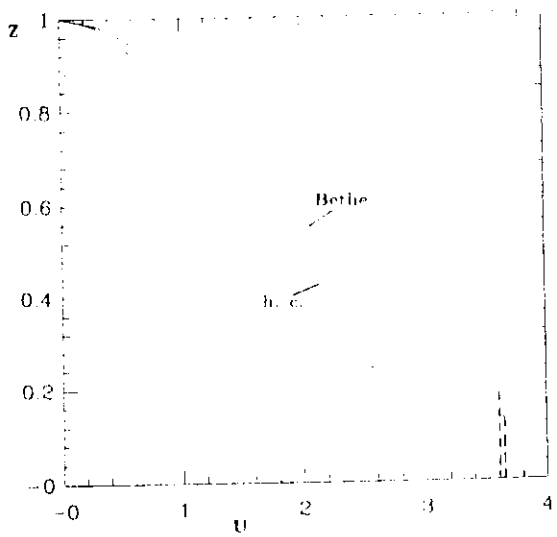

FIG. 8. Quasiparticle weight Z as a function of U for the hc lattice (lower curve) and Bethe lattice (upper curve), as obtained by IPT. Z directly yields the effective mass and spin-fluctuations scale (Kondo temperature) from $Z=m/m^*=T_F^*(U)/T_F^*(0)$. Note that the Gutzwiller approximation yields the straight line $Z_{GA}=1-U/U_{BR}$, with $U_{BR}=8\epsilon_0\simeq 4.5$ for the hc lattice ($\simeq 4.8$ for the Bethe lattice).

centered at $\omega=0$, and broad high-energy satellite peaks on a scale set by U. This parallels the above results for C_v.

As a consequence of the Luttinger theorem, the height of the quasiparticle peak remains equal to its free value independently of the interaction strength U.[13] Its width is set by the quasiparticle weight Z and is thus proportional to T_F^* (for the hc lattice, the width at half-height can be estimated as $\simeq 2\sqrt{\ln 2}Zt_*\simeq 1.66Zt_*\simeq 6T_F^*$). Note the following low-frequency expansion of $\rho(\omega)$ obtained by inserting (24) and (25) into (26):

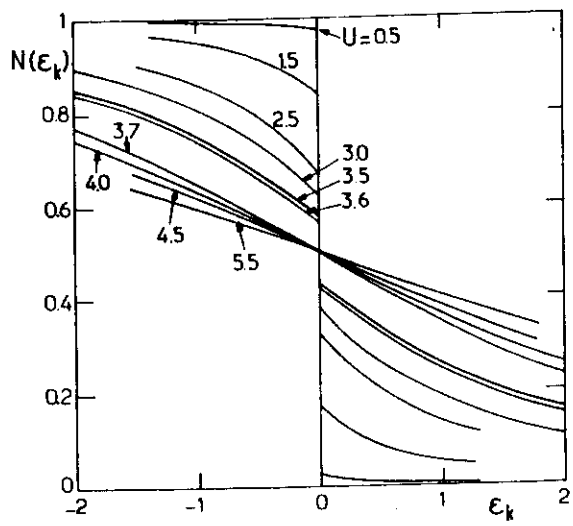

FIG. 9. Distribution of occupied states $N(\epsilon_k)$, for various values of U (hc lattice) within IPT. Note the absence of a jump for $U>U_c$ and the abrupt change of behavior above $U=3.6$.

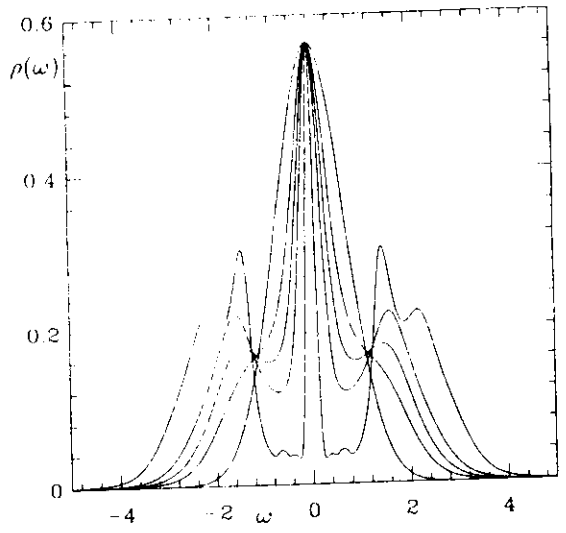

FIG. 10. IPT results for the local $T=0$ spectral density of the paramagnetic solution, $\rho(\omega)$ at $U=0$, 1.5, 2, 2.5, 3.65 (hc lattice).

$$\rho(\omega)=D(0)-\frac{1}{2}\omega^2\left[\frac{D_2}{Z^2}+\frac{2D_1\gamma}{\pi}\right]+O(\omega^4)\,, \qquad (27)$$

where $D_2=-D''(0)>0$ and $D_1=-\int d\epsilon\, D'(\epsilon)/\epsilon>0$ [$D(0)=1/\sqrt{\pi}$, $D_1=2$, $D_2=2/\sqrt{\pi}$ for the Gaussian DOS with $t_*=1$]. This shows that Z controls the curvature of the quasiparticle peak near $\omega=0$.

The satellite peaks can be interpreted as high-energy charge excitations signaling the formation of the upper Hubbard band. They are found to form already for moderate values of U,[3] both within the IPT scheme and when an analytic continuation is made on the exact enumeration results. This is in qualitative agreement with the results of straight $O(U^2)$ weak-coupling expansions,[28] but *not* with the self-consistent schemes of Refs. 29 and 30. The latter fail to reproduce the high-energy excitations correctly. Note that, for U large enough, we find that the upper Hubbard band acquires a two-peak structure. As discussed below, the lowest-frequency one can be viewed in a sense as a mirror image of the quasiparticle peak.

Let us mention that the overall shape of the spectral density and its dependence on U found here is in good qualitative agreement with recent photoemission experiments of several transition-metal oxides.[41]

Finally, we describe how the spectral density behaves for *finite* temperature. Figure 11 (a) illustrates the evolution of $\rho(\omega)$ when raising the temperature from $T=0$, with $U=3<U_c$. At a low-temperature scale given roughly by the half-width of ρ at $T=0$ (i.e., $\simeq 3T_F^*$), the quasiparticle peak is suppressed and the curvature of $\rho(\omega)$ near $\omega=0$ becomes negative. For completeness, we also display in Fig. 11(b) IPT results for $\rho(\omega)$ at a *fixed* temperature $\beta=7.2$, for increasing values of U. The same behavior is apparent. The curves in Fig. 11(b) agree very well with the results of Jarrell and Pruschke in Ref. 8 obtained by a maximal entropy continuation of Monte

Carlo data for the same parameters. This agreement gives us confidence in the accuracy of the IPT scheme.

C. Impurity-model interpretation: Local Kondo effect

The above properties have a simple interpretation[3] when following the analogy with a single-impurity Anderson model in the particle-hole symmetric case, described in Sec. II C. The important quantity to think about in this framework is the density of states of the effective conduction electron bath, $\Delta(\omega)$. Let us emphasize that, unlike the situation usually considered when discussing the one-impurity Anderson model, $\Delta(\omega)$ itself changes continuously with U here, and has strong frequency dependence as well. In the metallic phase, $\Delta(\omega=0)$ *remains finite* (and *independent of U*), while the width of $\Delta(\omega)$ around $\omega=0$ *decreases as U increases.*

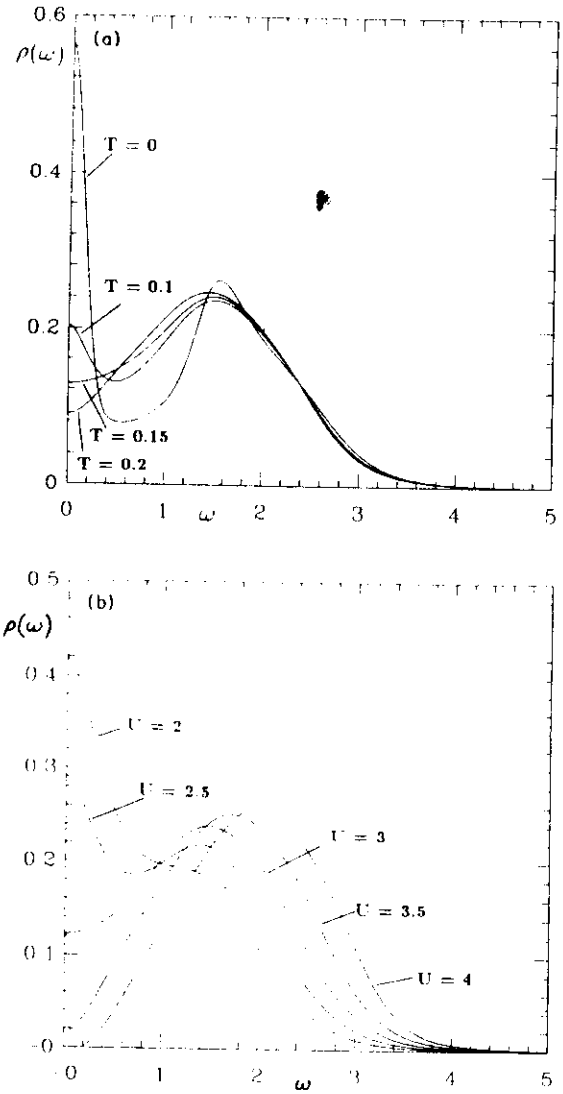

FIG. 11. (a) Local spectral density $\rho(\omega)$ at $U=3$ (hc lattice) for temperatures $T=0$, 0.1, 0.15, 0.2 (IPT method). The quasiparticle peak disappears at a scale set by T_F^*. (b) Local spectral density $\rho(\omega)$ at *finite temperature* $\beta=7.2$, for $U=2$, 2.5, 3, 3.5, 4 (IPT method). Very similar results were obtained in Ref. 8 using an analytic continuation of Monte Carlo data.

This is obvious for the Bethe lattice, for which $\Delta(\omega)=(t_*/\sqrt{2})^2\rho(\omega)$. More generally, it is apparent on the low-frequency expansion of $\Delta(\omega)$ obtained by making use of (24) and (25) into the self-consistency equation (6):

$$\Delta(\omega)=\Delta(0)+\Delta''(0)\omega^2/2+O(\omega^4)\ ,$$

with

$$\begin{aligned}\pi\Delta(0)&=\frac{1}{\pi D(0)}\ ,\\ \pi\Delta''(0)&=\frac{1}{[\pi D(0)Z]^2}\left[\pi D_2-\frac{2D_1^2}{\pi D(0)}\right]\\ &\quad+2\gamma\left[\frac{D_1}{[\pi D(0)]^2}-1\right]\quad(<0)\ .\end{aligned}\tag{28}$$

Since $\Delta(\omega)$ is nonzero around $\omega=0$, one has the familiar situation of a magnetic impurity in a metal. The single-site problem enters a Kondo regime upon increasing U, with almost frozen charge fluctuations and on-site spin fluctuations between the two states $|\uparrow\rangle$, $|\downarrow\rangle$. In this framework, the low-temperature scale T_F^* $[=Z3\Delta(0)/2]$ must be interpreted as the Kondo temperature below which these spin fluctuations are quenched by the Kondo effect. As emphasized by Langreth[39] and Nozieres,[40] the properties of the impurity model below T_F^* are those of a local Fermi liquid described above. The quasiparticle peak in $\rho(\omega)$ may be interpreted in this framework as the Abrikosov-Suhl resonance. As a first crude approximation, the broad satellite peaks associated with the upper Hubbard band can be thought of as a superposition with equal weight $\frac{1}{2}$ of the two magnetic Hartree-Fock solutions. Hence, the nontrivial frequency dependence of the upper Hubbard bands reflects the strong frequency dependence of $\Delta(\omega)$. In particular, the additional peak appearing close to U_c can be viewed as a mirror image of the quasiparticle peak within the upper Hubbard band (note that it disappears in the insulator, cf. Fig. 13). In a renormalization-group picture, the metallic phase corresponds to a flow towards small U (or large hopping t_*), i.e., to the usual scaling towards strong Kondo coupling.

D. Response to a uniform field: Absence of metamagnetism

To complete the discussion of the physical properties of the Fermi-liquid phase, we report some results on the response of this phase to a uniform magnetic field. This is motivated in particular by remarkable recent experiments on liquid ^{3}He,[42] which indicate a smooth saturation of the magnetization as a function of field, with a magnetic susceptibility *decreasing* with increasing field. In contrast, the Gutzwiller approximation predicts a strong metamagnetic behavior of the Fermi liquid close to U_c, with a susceptibility which *increases* with field and a finite critical field above which the system is fully polarized ($m=1$).[36,37] Accordingly, a Maxwell relation suggests that consistent finite-temperature generalizations of the Gutzwiller approximation should lead to a susceptibility *increasing* with temperature at low temperature.[37]

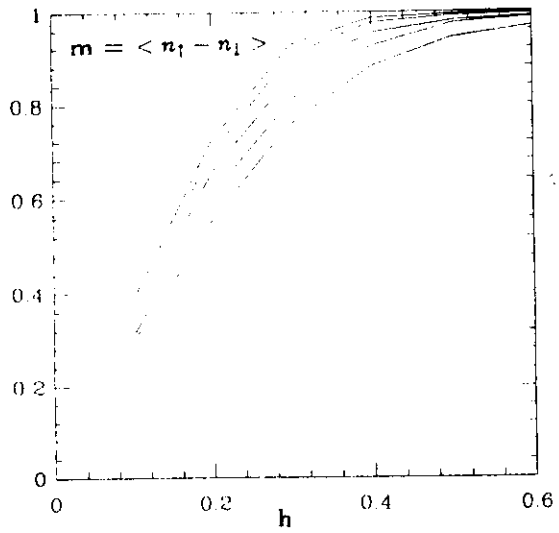

FIG. 12. Magnetization $m=\langle n_\uparrow - n_\downarrow \rangle$ vs applied uniform magnetic field h. From top to bottom: ($\beta=16$, $U=4$), ($\beta=16$, $U=3.5$), ($\beta=16$, $U=3$), ($\beta=8$, $U=3$), ($\beta=8$, $U=2.5$).

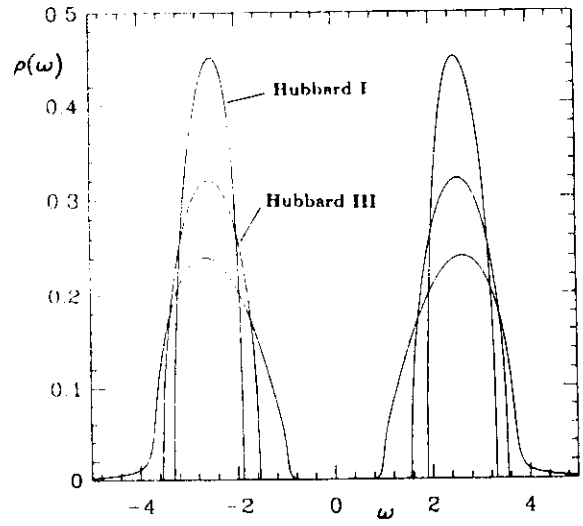

FIG. 13. Comparison of the IPT result for the $T=0$ local spectral density at $U=5$ (Bethe lattice) with the Hubbard I and Hubbard III approximations.

As explained above [Eq. (10)], the present method of solution is easily generalized to a uniform magnetic field h. Results obtained by exact enumeration with $L=16$ for the magnetization $m\equiv\langle n_\uparrow - n_\downarrow\rangle$ vs applied field, are displayed in Fig. 12 for $\beta=8$, $U=2.5$, 3 and $\beta=16$, $U=3$, 3.5, 4 (hc lattice). These results do not show any tendency to metamagnetic behavior. The magnetization smoothly saturates with field, and the susceptibility decreases upon increase of h. Comparison of the results for $U=3$ and $\beta=8$, 16 show that the susceptibility *decreases* with temperature. We also notice that, in contrast to the Gutzwiller approximation, the uniform susceptibility does not diverge as one crosses the metal-insulator transition (cf. Ref. 8).

These results show that the response to a uniform field is very poorly described by the Gutzwiller approximation. The underlying physical reason is that this approximation completely neglects charge fluctuations and residual magnetic exchange, which are of crucial importance for the magnetic properties of the true system.

VI. THE MOTT-HUBBARD LOCALIZED PHASE

A. Zero-temperature properties

Let us turn to the description of the insulating solution at zero temperature, found within the paramagnetic phase for $U>U_{c_1}$. A typical IPT result for $\rho(\omega)$ in this phase is displayed in Fig. 13. The spectrum is purely incoherent, with no quasiparticle peak ($Z=0$). The upper Hubbard bands are not found to display any remarkable structure in the insulator, in contrast to the vicinity of the transition on the metallic side. For the Bethe lattice, one has a finite Mott-Hubbard gap Δ_g. For the hypercubic lattice, only a pseudogap is found, with $\rho(\omega)$ vanishing as $\omega\to 0$, but finite for all nonzero frequency. This is expected from the existence of tails extending from $-\infty$ to $+\infty$ in the $U=0$ Gaussian DOS: arbitrarily low-energy excitations (with very small weight) must always exist in that case. They correspond to the exponentially small fraction of electrons which live in the tails of the DOS and have an arbitrarily large (negative) kinetic energy. A simple argument suggests that $\rho(\omega)$ vanishes as e^{-1/ω^2} for small ω in this case. Note, however, that, despite this peculiarity, there is a clear sense in which a Mott transition arises also for the hypercubic lattice.

The self-energy itself has a markedly different behavior from the Fermi-liquid one. Let us concentrate for simplicity on the Bethe lattice for which the self-consistency equation (9) implies $\Sigma(\omega+i0^+)=\omega-t_*^2 G/2-1/G$. It follows from this equation that $\Sigma(\omega+i0^+)$ must be real inside the gap [since there $\rho(\omega)=-1/\pi\,\mathrm{Im}G=0$], except for a δ-function piece in $\mathrm{Im}\Sigma$ at $\omega=0$:

$$\mathrm{Im}\Sigma(\omega+i0^+)=0 \quad \text{for } \omega\in[-\Delta_g/2,\Delta_g/2],\quad \omega\neq 0 \tag{29}$$

and that $\mathrm{Re}\Sigma$ has the following low-frequency behavior:

$$\mathrm{Re}\Sigma(\omega+i0^+)=\frac{1}{\omega}\left[\int_{-\infty}^{+\infty} d\epsilon\,\frac{\rho(\epsilon)}{\epsilon^2}\right]^{-1}+O(\omega)\ . \tag{30}$$

A typical IPT result for $\mathrm{Re}\Sigma$, $\mathrm{Im}\Sigma$ is displayed in Fig. 14 for the Bethe lattice with $U=5$.

B. Comparison with Hubbard I and III approximations

It is of interest to compare the actual results for the spectral density to the predictions of the first approximate treatments included in Hubbard's original papers.

The simplest and crudest approximations (known as Hubbard I) amounts to replacing the self-energy with its atomic limit in the Green's function:[12]

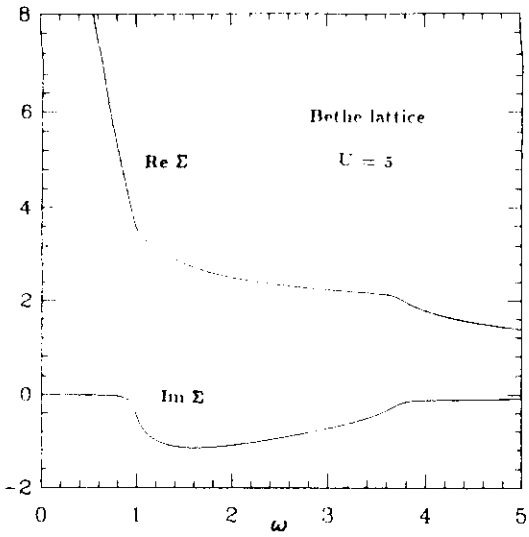

FIG. 14. $\mathrm{Re}\Sigma(\omega+i0^+)$ and $\mathrm{Im}\Sigma(\omega+i0^+)$ in the Mott-Hubbard phase at $U=5$ (Bethe lattice).

$$\text{Hubbard I:}\quad G(\mathbf{k},i\omega_n)=\frac{1}{i\omega_n-\epsilon_k-U^2/4i\omega_n}\ ,$$

$$\text{i.e.,}\quad \rho(\omega)=D\left[\omega-\frac{U^2}{4\omega}\right]\ . \tag{31}$$

This expression incorrectly predicts an insulating solution with a gap for arbitrarily small values of $U>0$. It is compared to the actual $\rho(\omega)$ in Fig. 13 for $U=5$.

A more refined approximation is known as Hubbard III.[43] As recently emphasized in Ref. 10, it is easily understood on the mean-field equations (5) and (6). It amounts to solving in an approximate manner the single-site action (5), thinking of G_0^{-1} as an *almost local function of time*. Hence, the interacting Green's function of $\mathcal{S}$ is approximated by

$$G(i\omega_n)\simeq\frac{1}{2}\left[\frac{1}{\hat{G}_0(i\omega_n)^{-1}-U/2}+\frac{1}{\hat{G}_0(i\omega_n)^{-1}+U/2}\right]\ . \tag{32}$$

This is then used in the self-consistency condition (6) to get a closed equation for G, which reads

Hubbard III:

$$G(i\omega_n)=\tilde{D}\left[i\omega_n-\frac{1}{2G}[\sqrt{1+U^2G^2}-1]\right]\ . \tag{33}$$

For the Bethe lattice, this equation can be simplified into[10]

Hubbard III (Bethe lattice):

$$\tfrac{1}{4}G^3-\omega G^2+\left[\omega^2+\frac{2-U^2}{4}\right]G-\omega=0\ . \tag{34}$$

This equation does lead to a metal-insulator transition at $U_c^{\mathrm{III}}=\sqrt{2}t_*$. The corresponding $\rho(\omega)$ is also displayed in Fig. 13. Qualitatively, this approximation describes correctly the insulating regime, as recently emphasized in Ref. 10. Indeed, for very large U/t_*, G_0^{-1} does become local and the Hubbard III approximation provides a quick way to show that the paramagnetic solution must be insulating for large U. It fails completely on the metallic side, however, since it neglects all coherence effects. Quantitatively, it is clear from Fig. 13 that both the Hubbard I and Hubbard III approximations are quite inaccurate.

C. Thermodynamic and magnetic properties: Physical nature of the localized phase

Figure 15 displays specific-heat curves for the paramagnetic solution in the localized regime with increasing values of U (Bethe lattice). They have the expected activated behavior $\sim e^{-\Delta_g/T}$ at low temperature, and a broad maximum at high temperature associated with charge fluctuations involving the upper Hubbard band.

The entropy can also be obtained using Eq. (22), and is displayed in Fig. 16 for $U=5$. Remarkably, a residual entropy is found at zero temperature, with $S(T=0)$ very close to the value $N\ln 2$. This would be easy to understand in an oversimplified description of the localized phase, pictured as a collection of independent magnetic moments, as, e.g., in the Gutzwiller approximation. In the present context, however, it is surprising at first sight since the $d\to\infty$ limit does not neglect charge fluctuations and residual magnetic exchange. One must realize, however, that there are actually *two different exchange scales* in this limit: one is the exchange coupling between two fixed spins $J_{ij}\sim t_{ij}^2/U\sim O(1/d)$ while the other is the exchange energy between a spin and its shell of d antiparallel neighbors. Since the latter is d times the former, it remains $O(1)$ and sets the scale for the Néel temperature. The first scale does vanish as $d\to\infty$, and controls the splitting between singlet states with total $S_z=0$. Hence, the $d\to\infty$ limit *does lead to a degenerate ground state* if one insists on singlet states without long-range magnetic order, as discussed here.[44] This is especially clear for the fully connected random model mentioned in Sec. IV [Eq. (21)], whose ground state is the paramagnetic insulator. For this model, the ground state for $U\to\infty$ is the highly degenerate set of total singlet states ($\sum_{i=1}^{N}S_i^z=0$).

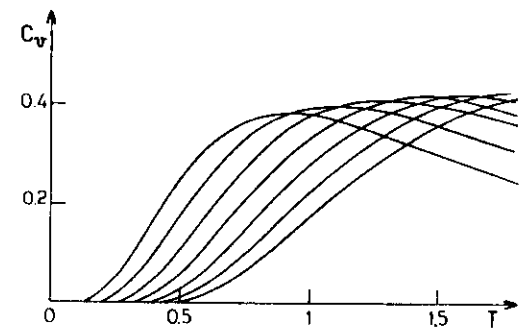

FIG. 15. Specific heat vs temperature of the paramagnetic solution in the insulating regime, for $U=4, 5, 6, \ldots, 10$.

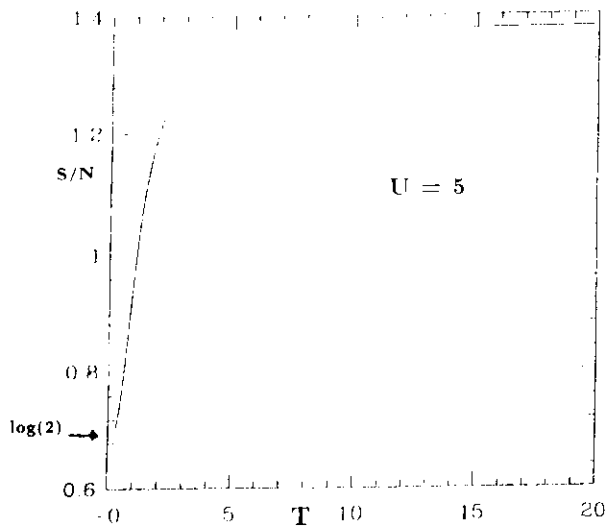

FIG. 16. Entropy per lattice site, S/N vs temperature, for $U=5$. Note the residual entropy $\sim \ln 2$ at $T=0$.

Note, furthermore, that the uniform magnetic susceptibility of the localized phase is finite and set by the $O(1)$ exchange scale. This is clearly seen in the numerical results of Fig. 12 for $U=4$. As a final evidence that the $d \to \infty$ limit does include charge fluctuations, we emphasize that the results of Fig. 6 for the fraction of doubly occupied sites show that $\langle D \rangle$ does not vanish even at zero temperature in this phase (as it would in the Gutzwiller approximation). Obviously, $\langle D(T=0) \rangle$ is not an order parameter of the Mott transition. We also notice that the $\langle D \rangle$ vs T curves do not seem to display a minimum for $U > U_c$, in contrast to the metallic phase. (For $U=4$, we have performed simulations down to $\beta=32$, without observing a minimum.) This is in agreement with the spin-entropy interpretation of this minimum given in Sec. V A.

D. Impurity-model interpretation

The localized phase has a simple interpretation in the impurity-model framework. Clearly, the effective conduction bath DOS $\Delta(\omega)$ itself develops a gap (or a pseudogap for the hypercubic lattice). The situation is analogous to a magnetic impurity in an insulator. The Kondo effect does not take place in that case, since no conduction states are present near $\omega=0$. The Kondo quasiparticle peak is absent, and the special density has a gap. In a renormalization-group picture, this situation corresponds to a flow towards *weak* Kondo coupling ($\sim t_*^2/U$), i.e., towards large U (or small hopping t_*). Hence, a local moment remains down to zero temperature. A simple argument can be given[9,10] which shows that the Fermi-liquid regime of the paramagnetic solution must indeed be unstable at large enough values of U. We imagine solving the impurity model iteratively, as in our algorithm. At the nth step of the iteration, $G_0^{(n)}$ is characterized by the spectral density $\Delta^{(n)}(\omega)$, which possibly has $\Delta^{(n)}(0) \neq 0$ and a nonzero width $W^{(n)}$ around $\omega=0$. In the first step of the algorithm, the impurity model is solved given $\Delta^{(n)}(\omega)$ to yield a local spectral density $\rho^{(n+1)}(\omega)$. The quasiparticle peak in $\rho^{(n+1)}$ has a width $T_K(W^{(n)},U)$ (Kondo temperature) which is a function of U and of the width of $\Delta^{(n)}$. In the second step of the iteration, the self-consistency condition is used to produce an updated $\Delta^{(n+1)}$, which reads (for the Bethe lattice) $\Delta^{(n+1)}=t_*^2\rho^{(n+1)}/2$. Hence, the new width $W^{(n+1)}$ is essentially given by $T_K(W^{(n)},U)$. Thus, when U is large, $W^{(n)}$ is *decreased upon iteration*, and one quickly reaches a regime in which it becomes smaller than the other energy scales. Using the relevant expression for $T_K(W,U)$ in this regime obtained by Haldane's renormalization-group analysis,[48] one gets

$$W^{(n+1)} \simeq W^{(n)} \sqrt{\Delta(0)/U} \exp[-U/\Delta(0)] .$$

Hence, for U large enough, $W^{(n)}$ is decreased at each step of the iteration and must converge to $W^{(\infty)}=0$. This signals the opening of a gap in $\Delta(\epsilon)$, and shows that the Fermi-liquid phase is indeed unstable for U very large.

E. Nature of the Mott transition

As explained in Sec. IV, an insulating solution of the paramagnetic equations in the IPT approximation exists for $U > U_{c1}$, while a metallic solution exists[11] for $U < U_{c2}$, with $U_{c1} < U_{c2}$, at $T=0$. The physical mechanism responsible for these two transitions are quite different. At U_{c2},[49] the quasiparticle residue $Z \simeq T_K$ vanishes continuously, hence destroying the coherence of the metal. This transition follows to some extent the Brinkman-Rice (BR) scenario,[47,36,37] with a diverging effective mass $m^*/m = 1/Z$. The *uniform* magnetic susceptibility does not diverge, however (hence the Wilson ratio *vanishes*), in contrast to the BR description which neglects exchange and charge fluctuation effects. Note that the BR value for U_{c2} (based on the Gutzwiller approximation) reads $U_{BR}=8\epsilon_0 \simeq 4.5 t_*$ ($\simeq 4.8 t_*$ for the Bethe lattice), close to the value found within IPT.[11] Moreover, the Gutzwiller result for the quasiparticle residue $Z=1-U/U_{BR}$ is not a bad description of the results of Fig. 8.

However, within IPT this continuous transition is preempted by the appearance of an insulating solution for $U > U_{c1}$, with $U_{c1} < U_{c2}$. This is quite unrelated to low-frequency coherence effects, but rather is a high-energy effect. It is due to the existence, at large enough U, of two degenerate magnetic solutions of the impurity problem at the Hartree-Fock level. The Mott insulating state is built from an incoherent superposition of these solutions. The insulating gap closes continuously at U_{c1}. This transition is qualitatively similar to the rigid-band picture of the Hubbard III approximation.

It results from the above that a region of coexistence is found in the (U,T) parameter space (Fig. 2) and that the Mott transition is found to be first order within IPT (see also Ref. 11). We find within IPT, at all temperatures that we studied ($T > 0.01$), that the insulating solution has lower free energy (due to the residual entropy $\simeq N \ln 2$), even though the internal energies are quite close. The actual critical line $U_c(T)$ is thus very close to the lower boundary of the coexistence region (Fig. 2).

VII. THE ANTIFERROMAGNETIC PHASE

In Secs. V and VI, we have described the behavior of the solution of the paramagnetic equations (5) and (6). On bipartite lattices, this corresponds to the actual equilibrium state of the model only for large enough temperatures. When the full set of equations (11) is solved, allowing for spin and translational symmetry breaking, the numerical results do converge towards the paramagnetic solution above the Néel temperature $T_N(U)$,[46] while a solution with long-range antiferromagnetic order is found for $T < T_N$. In Fig. 17 we show results obtained by exact enumeration ($L=16$) for the Green's functions on the hc lattice with $U=2.5$, $\beta=8$ [note that $G_{A,\sigma}(\tau)=G_{B,-\sigma}(\beta-\tau)$ at half filling]. Using this full algorithm, the Néel temperature can be calculated as a function of U together with the staggered magnetization in the antiferromagnetic phase from

$$m_s=\langle n_{\uparrow,A}-n_{\downarrow,A}\rangle=1+2G_{\uparrow,A}(\tau=0^+)\ .$$

We have calculated the Néel temperature as a function of U from both an extrapolation of $m_s(T)$ and the test of local stability of the paramagnetic solution.[45] The results were given on the phase diagram of Fig. 2 (Sec. IV): $T_N(U)$ is a maximum for $U\simeq 3$ and never exceeds ~ 0.14.

Figure 18 displays the staggered magnetization as a function of temperature for $U=2.5$ on the hc lattice. We find the Néel temperature to be $T_N(U=2.5)=0.13\pm 0.01$. This value agrees very well with Ref. 8, obtained by a different method based on the calculation of the staggered susceptibility. It was also noticed in Ref. 8 that recent Monte Carlo results for the $d=3$ case agree quite well with the $d\to\infty$ limit.

We have also investigated the IPT approximation in the antiferromagnetic phase: a comparison is made in Fig. 17. The agreement with the numerical solution is, by

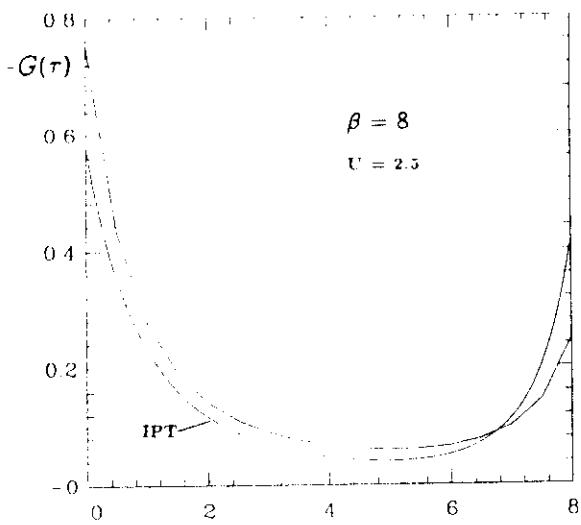

FIG. 17. Local Green's function $G_{A,\uparrow}(\tau)$ in the antiferromagnetic phase at $\beta=8$, $U=2.5$ (hc lattice). Upper curve: exact enumeration results. Lower curve: IPT approximation. Note that the latter underestimates m_s.

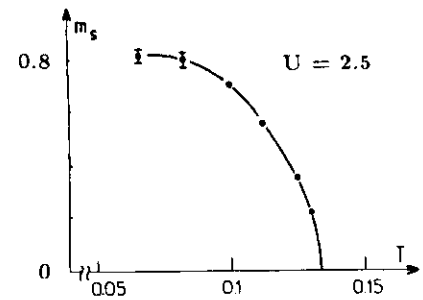

FIG. 18. Staggered magnetization m_s vs temperature at $U=2.5$.

far, not as good as in the paramagnetic case. The overall behavior of the Green's functions is qualitatively correct and the Néel temperature well approximated, but the staggered magnetization is not.

Finally, we have also determined the specific heat in the antiferromagnetic phase as a function of temperature. We find an activated behavior at low temperature, $\sim e^{-\Delta/T}$. This is expected from the fact that $d\to\infty$ is a mean-field limit in which spin-wave excitations are suppressed. Accordingly, C_v becomes very large close to T_N, and has a discontinuity at T_N. Above this discontinuity, the results of Figs. 4 and 15 are recovered. The large discontinuity is such that both the paramagnetic and antiferromagnetic solutions have the same integrated value for the entropy at T_N.

VIII. CONCLUSION

We have presented in this paper a detailed study of the physical properties of the $d=\infty$ Hubbard model at half filling, using a previously introduced numerical method to solve the exact mean-field equations satisfied by the Green's functions in this limit. Two equilibrium phases are found: a two-sublattice antiferromagnet at low temperature and a paramagnetic phase. In addition, the paramagnetic equations display a phase transition between a paramagnetic metal (Fermi liquid) for weak coupling and a paramagnetic Mott-Hubbard insulator for strong coupling. This transition can also be seen as a true ground-state phase transition for a fully connected Hubbard model with randomness on the hopping parameters.[31]

The nature of this transition within IPT is found to be more complex than suggested by many other approximate descriptions such as the Brinkman-Rice[47] and Hubbard approximations. We find (see also Ref. 11) a region of coupling and temperature in which two solutions of the mean-field equations coexist, from which we infer the existence of a first-order transition line extending to low but finite temperature. Both charge and spin *local* fluctuations are retained in the $d=\infty$ limit. As a result, we find no divergence of the *uniform* magnetic susceptibility at the transition and in the insulating phase, and no tendency to metamagnetism. The insulating phase does correspond, however, to the formation of local moments, and has (for $d=\infty$) a residual ground-state entropy. The IPT scenario of a first-order transition remains to be

verified in the full numerical solution of the mean-field equations.

We have also presented numerical results for several thermodynamic quantities (specific heat, entropy, density of doubly occupied sites) as a function of temperature. In the metallic regime, the results reflect the gradual separation of two energy scales: a low-energy scale associated with local spin fluctuations (corresponding to the Kondo scale in the associated single-impurity model) and a high-energy scale associated with charge fluctuations. The first scale disappears in the Mott insulator.

Finally, we have shown that a numerical solution of the $d=\infty$ Hubbard model can also be achieved within the long-range ordered antiferromagnetic phase, and have presented results for the staggered magnetization as a function of temperature.

All these results demonstrate that a detailed quantitative understanding of strongly correlated fermion models can be achieved in the limit of infinite spatial dimensionality. The crucial physics of local spin and charge fluctuations is kept in this limit, leading to a rich variety of physical behavior. We believe that direct extensions of the present work may improve our understanding of physical systems such as liquid ^{3}He and Mott insulators. Other strongly correlated fermion models, such as the Kondo and Anderson lattices, are currently under investigation using the same methods. $d=\infty$ is also, in a sense, the simplest of all dimensions for the numerical study of fermionic lattice problems, since the problem is reduced to the solution of a self-consistent single-impurity model with no spatial degrees of freedom.

The $d=\infty$ limit does have some limitations however. In our opinion, the main one is the complete freezing of long-wavelength *spatial* fluctuations (such as, e.g., spin-wave modes), in contrast to *temporal* fluctuations which are treated exactly. It would be extremely interesting to find a theoretical scheme to include these fluctuations into the present framework, such as some kind of loop expansion around $d=\infty$.

ACKNOWLEDGMENTS

We would like to thank G. Kotliar, S. Sachdev, P. Nozieres, and D. S. Fisher for contributing very helpful remarks. We are also indebted to J. P. Bouchaud, J. K. Freericks, F. D. M. Haldane, M. Rozenberg, Q. Si, and X. Y. Zhang for interesting discussions. A.G. would like to thank G. Kotliar for collaboration and sharing many insights, and acknowledges the hospitality of Rutgers University, the Institute for Theoretical Physics in Santa Barbara (under NSF Grant No. PHY89-04035), and the International Center for Theoretical Physics in Trieste at various stages of this work. We recently received a copy of unpublished work by Pruschke *et al.*[50] which has some overlap with the present results and also investigates transport properties. Laboratoire de Physique Théorique is Unité propre du CNRS (UP 701) associée à l'ENS et à l'Université Paris-Sud. Laboratoire de Physique Statistique is Laboratoire associé au CNRS (URA 1306) et aux Universités Paris VI et Paris.

*Electronic address: GEORGES@PHYSIQUE.ENS.FR
†Electronic address: KRAUTH@PHYSIQUE.ENS.FR

[1]W. Metzner and D. Vollhardt, Phys. Rev. Lett. **62**, 324 (1989).
[2]For a recent review and references, see, e.g., D. Vollhardt, in *Correlated Electron Systems*, Proceedings of the Jerusalem Winter School of Theoretical Physics, edited by V. J. Emery (World Scientific, Singapore, in press).
[3]A. Georges and G. Kotliar, Phys. Rev. B **45**, 6479 (1992).
[4]A. Georges, G. Kotliar, and Q. Si, Int. J. Mod. Phys. B **6**, 705 (1992).
[5]P. van Dongen and D. Vollhardt, Phys. Rev. Lett. **65**, 1663 (1990).
[6]V. Janis, Z. Phys. B **83**, 227 (1991).
[7]The first detailed study of these mean-field equations was performed by U. Brandt and C. Mielsch, Z. Phys. B **75**, 365 (1989); **79**, 295 (1990); **82**, 37 (1991), in the restricted case $t_\uparrow \neq t_\downarrow = 0$ (Falicov-Kimball model), for which an exact solution is possible.
[8]M. Jarrell, Phys. Rev. Lett. **69**, 168 (1992); M. Jarrell and T. Pruschke (unpublished).
[9]A. Georges and W. Krauth, Phys. Rev. Lett. **69**, 1240 (1992).
[10]M. Rozenberg, X. Y. Zhang, and G. Kotliar, Phys. Rev. Lett. **69**, 1236 (1992).
[11]X. Y. Zhang, M. Rozenberg, and G. Kotliar, Phys. Rev. Lett. **70**, 1666 (1993); and (unpublished).
[12]J. Hubbard, Proc. R. Soc. London Ser. A **276**, 238 (1963).
[13]E. Muller-Hartmann, Z. Phys. B **74**, 507 (1989).
[14]They can, however, be considered as a mean-field *approximation* in more general instances, with an arbitrary DOS $D(\epsilon)$: it amounts to ignoring momentum conservation in all *skeleton* diagrams for the self-energy, while retaining frequency conservation.
[15]A useful numerical algorithm for the complex error function has been published as "algorithm 680, collected algorithms from ACM," [Transact. Math. Software **16**(1), 47]. We are grateful to J. K. Freericks for pointing this out to us.
[16]B. Horvatic and V. Zlatic, Solid State Commun. **75**, 263 (1990).
[17]See, e.g., A. L. Fetter and J. D. Walecka, *Quantum Theory of Many-Particle Systems* (McGraw-Hill, New York, 1971). As written, this formula is particularly well suited to deal with numerical frequency summations since all terms decay faster than $1/\omega$.
[18]P. W. Anderson, Phys. Rev. **124**, 41 (1961).
[19]P. A. Wolf, Phys. Rev. **124**, 1030 (1961).
[20]In actual computations, we take for $G(i\omega_n)$ the Fourier transform of a function constructed from the points $G(\tau_i)$ by a spline interpolation and such that it has the correct amplitude of the jump at $\tau=0$: $G(\tau=0^+)-G(\tau=0^-)=-1$.
[21]G_0 is self-consistently determined and does not have, in general, the form corresponding to the integrable case for the impurity model, except for a very special (Lorentzian) choice of the DOS $D(\epsilon)$, which has rather nongeneric properties: see Refs. 3 and 4.
[22]J. E. Hirsch and R. M. Fye, Phys Rev. Lett. **56**, 2521 (1986).
[23]R. Blankenbekler, D. J. Scalapino, and R. L. Sugar, Phys. Rev. D **24**, 2278 (1981).
[24]The enumeration proceeds as $(\cdots -1,-1,-1,-1)$, $(\cdots -1,-1,-1,+1)$, $(\cdots -1,-1,+1,+1)$, $(\cdots -1,-1,+1,-1)$, etc. See E. M. Reingold, J. Niever-

gelt, and N. Deo, *Combinatorial Algorithms, Theory and Practice* (Prentice Hall, Englewood Cliffs, NJ, 1977).

[25]H. J. Vidberg and J. W. Serene, J. Low Temp. Phys. **29**, 179 (1977).

[26]The final results for physical quantities are obtained by extrapolating to small $\Delta\tau(L\to\infty)$. For the range of parameters studied, this turned out to be safely possible provided $\Delta\tau$'s of order 0.5 are reached.

[27]K. Yosida and K. Yamada, Prog. Theor. Phys. **46**, 244 (1970); **53**, 1286 (1975); K. Yamada, *ibid.* **53**, 970 (1975); V. Zlatic, B. Horvatic, and D. Sokvecic, Z. Phys. B **59**, 151 (1985); M. Salomaa, Solid State Commun. **39**, 1105 (1981).

[28]H. Schweitzer and G. Czycholl, Z. Phys. B **83**, 93 (1991).

[29]E. Muller-Hartmann, Z. Phys. B **76**, 211 (1989).

[30]B. Menge and E. Muller-Hartmann, Z. Phys. B **82**, 237 (1991).

[31]This has been established in a joint work with S. Sachdev. We are also indebted to D. S. Fisher for very useful remarks on this point.

[32]Note that this fully connected model can be solved analytically in the absence of randomness, see P. Van Dongen and D. Vollhardt, Phys. Rev. B **40**, 7252 (1989).

[33]More precisely, denoting by $E(\beta,L)$ the internal energy for a given inverse temperature and grid size, we compute C_v as $C_v(\beta=L\Delta\tau,\Delta\tau)=E(L\Delta\tau,L)-E[(L+1)\Delta\tau,L+1]/(L\Delta\tau)^{-1}-[(L+1)\Delta\tau]^{-1}$, and extrapolate for $\Delta\tau\to 0$.

[34]D. S. Greywall, Phys. Rev. B **27**, 2747 (1983).

[35]K. Seiler, C. Gros, T. M. Rice, K. Ueda, and D. Vollhardt, J. Low Temp. Phys. **64**, 195 (1986).

[36]D. Vollhardt, Rev. Mod. Phys. **56**, 99 (1984).

[37]See, e.g., P. Nozieres (unpublished).

[38]D. B. McWhan, J. P. Remeika, T. M. Rice, W. F. Brinkman, J. P. Maita, and A. Menth, Phys. Rev. Lett. **27**, 941 (1971).

[39]D. Langreth, Phys. Rev. **150**, 516 (1966).

[40]P. Nozieres, J. Low Temp. Phys. **17**, 13 (1975).

[41]A. Fujimori, I. Hase, H. Namatame, Y. Fujishima, Y. Tokura, H. Eisaki, S. Uchida, K. Takegahara, and F. M. F. de Groot, Phys. Rev. Lett. **69**, 1796 (1992).

[42]S. Wiegers, P. E. Wolf, and L. Puech, Phys. Rev. Lett. **66**, 2895 (1991).

[43]J. Hubbard, Proc. R. Soc. London Ser. A **281**, 401 (1964).

[44]We thank D. S. Fisher and P. Nozieres for clarifying discussions on this point.

[45]The convergence is slow close to T_N, and can be sped up tremendously using standard methods of acceleration of slowly converging series. We have used the Shanks transform described in C. M. Bender and S. A. Orszag, *Advanced Mathematical Methods for Scientists and Engineers* (McGraw-Hill, New York, 1978), p. 396 ff.

[46]For some values of U, T, a modified update formula has been used in order to avoid cycles in the algorithm, e.g., $G_{0,\text{new}}=1/2[G_0+\tilde{D}(i\omega_n-\Sigma)]$.

[47]W. F. Brinkman and T. M. Rice, Phys. Rev. B **2**, 4302 (1970).

[48]F. D. M. Haldane, Phys. Rev. Lett. **40**, 416 (1978); Ph.D. thesis, University of Cambridge, 1977 (unpublished).

[49]For recent analytic insights into this transition, see Ref. 11 and D. S. Fisher (unpublished).

[50]T. H. Pruschke, D. L. Cox, and M. Jarrell (unpublished).

THE MOTT TRANSITION IN INFINITE DIMENSIONS: OLD IDEAS AND SOME SURPRISES

Gabriel Kotliar and Marcelo J. Rozenberg*

Department of Physics, Rutgers University, Piscataway, NJ 08855, USA

The Mott transition phenomena can be studied systematically in the limit of large dimensions. We describe recent results and new insights in this field.

1. Introduction

The Mott transition, namely the metal insulator transition induced by the electron electron interactions in a periodic system, has been investigated theoretically and experimentally for many years [1]. Experimentally it is realized in transition metal oxides such as V_2O_3 and NiI_2 and can be driven by varying pressure, temperature and composition. The Mott transition inspired the development of many important theoretical concepts. Hubbard introduced the notion of Hubbard bands, and view the metal insulator transition as a gradual merging of these bands as the correlation is decreased. Brinkman and Rice viewed the metal insulator transition as a result of a collapse of the Fermi energy or the divergence of the effective mass a critical value of the interaction U. In this framework the metal insulator transition is driven by the disappearance of the Fermi liquid quasiparticles. Slater pointed out that the metal insulator transition is always accompanied by long range antiferromagnetic order, and viewed the doubling of the unit cell which makes the band structure of the system that of a band-insulator, as the driving force behind the metal insulator transition.
These ideas and the relevance of the Hubbard model as a simple model to account for the essential features displayed by real systems have been debated for a long time.
The interest in the quantum many body problem in the limit of infinite dimensions [2], has led to a new mean field theory of the strong correlation problem [3,6]. This theory is similar in spirit to the Weiss mean field theory in classical statistical mechanics. It has given new insights into the Mott transition problem [7,12] and describes quantitatively some recent experiments on three dimensional transition metal oxide systems [12]. We will review here some of these developments.
Our starting point is the Hubbard Model:

$$H = -\sum_{<i,j>}(t_{ij}+\mu)c^{\dagger}_{i\sigma}c_{j\sigma} + U\sum_{i}(n_{i\uparrow}-\frac{1}{2})(n_{i\downarrow}-\frac{1}{2}), \tag{1}$$

where summation over repeated spin indices is assumed.
In the limit of the coordination number m going to infinity, the hopping matrix elements can be chosen to give a semicircular density of states of width $4t$, and are scaled as $t_{ij} \sim \frac{t}{\sqrt{m}}$ [2] to give a well defined and non trivial limit. This density of states is realized on lattices with different amounts of magnetic frustration such as the Bethe lattice (no frustration), the fully connected - fully frustrated lattice

(FF) [10], and the two sublattice fully frustrated model (TSFF), which provides a varying degree of frustration [12].
More precisely the models are defined as follows: in the first case the parameters t_{ij} for $n.n.$ hopping are chosen equal to a constant t. In the second case, the t_{ij} are chosen as a random variable with gaussian distribution, with zero mean and variance equal to t^2. In the third model we consider two sublattices. Each one fully connected, with hopping parameters chosen as in the previous case, but with variance equal to t_1^2. The hopping between sites on the different sublattices is given by $t_2 = \sqrt{t^2 - t_1^2}$.
Magnetic frustration is essential for the Mott phenomena and the study of lattices with varying degrees of frustrations allowed us to understand the interplay of the metal insulator transition and magnetic order.

2. Methodology

The essential idea of the mean field approach is to replace the quantum many body problem by a single site problem (impurity model) in an effective medium which is solved for self consistency [3] [6].
For the Hubbard model the associated impurity model is an Anderson model defined by the effective action:

$$S_{eff}[c, c^\dagger] = \sum_\sigma \int d\tau d\tau' c_\sigma^\dagger(\tau) G_0^{-1}(\tau - \tau') c_\sigma(\tau') + U \int_0^\beta d\tau (n_{i\uparrow}(\tau) - \frac{1}{2})(n_{i\downarrow}(\tau) - \frac{1}{2}). \tag{2}$$

The propagator G_0 plays the role of a Weiss field and, restricting to the paramagnetic phase (or for the FF model), obeys the self-consistency condition:

$$G_0^{-1}(i\omega_n) = i\omega_n + \mu - t^2 G(i\omega_n) \tag{3}$$

where $G(i\omega_n) = -\int_0^\beta e^{i\omega_n \tau} < T_\tau c(\tau) c^\dagger(0) >_{S_{eff}}$ is the local Green function of the Hubbard model once self-consistency is attained.
The mean field approach can be also used to investigate the occurrence of magnetic long range order. [6] To allow for an antiferromagnetic state on a bipartite lattice such as the Bethe lattice, the local Green functions and the Weiss fields are allowed to be spin dependent $G_{A\sigma} = G_{B-\sigma}$. This results in a different self consistency condition:

$$G_{0A\sigma}^{-1} = i\omega + \mu - t^2 G_{B\sigma} \tag{4}$$
$$G_{0B\sigma}^{-1} = i\omega + \mu - t^2 G_{A\sigma} \tag{5}$$

where A denotes one sublattice and B the other. The two impurity Green's functions G_A and G_B are evaluated independently given $G_{0A\sigma}$, $G_{0B\sigma}$ and the single site action S defined above.
The TSFF model that actually interpolates between the previous two, has a self consistency condition that reads

$$G_{0A\sigma}^{-1} = i\omega + \mu - t_1^2 G_{A\sigma} - t_2^2 G_{B\sigma} \tag{6}$$
$$G_{0B\sigma}^{-1} = i\omega + \mu - t_1^2 G_{B\sigma} - t_2^2 G_{A\sigma} \tag{7}$$

This model mimics a partial degree of frustration; it reduces to the Bethe lattice when $t_1 = 0$ and to the FF when $t_1 = t_2$.
The mean field equations are coupled functional equations to be solved for the Weiss field G_0 and the local Green function. The most difficult aspect of the mean field theory is the solution of the Anderson impurity model in an arbitrary bath. This class of problems has been studied intensively in the last 40 years and we will draw on this knowledge to make exact and approximate statements on the solution of the lattice model in large dimensions. The essential insight is to use ***reliable*** approximations to calculate $G\{G_0\}$ in eq. (2), this step captures the local aspects of the problem. The self consistency condition (3) then brings back the lattice aspect.
Several techniques have been used in the analysis of the mean field equations. They range from qualitative arguments and analytic perturbative schemes to numerical methods based on quantum Montecarlo (QMC) [7,9], exact diagonalization (ED) [14] [16] and second order perturbative calculations (2OPT) [10,12]. To obtain details of the low energy behavior we have developed the projective self-consistent method which is the lattice equivalent for large d problems of the Wilson renormalization group method [15]. An important point here is that no single technique can be pointed out as the most suitable, but the insights obtained on the Mott transition problem rely on a combined use of these techniques to elucidate the different aspects of the physics. We will illustrate the capabilities and the range of applicability of the different approaches in the following sections where we present the results for the model. Throughout the paper, we take the half-bandwidth $D = 2t = 1$.

3. Mott Transition at Half Filling

The schematic (from 2OPT) phase diagram of the Hubbard model at half filling in a fully frustrated lattice is shown in figure 1.

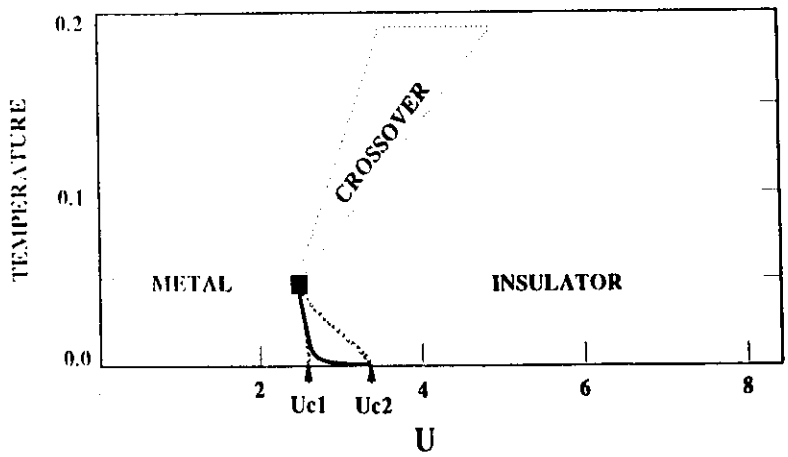

FIG. 1. Phase diagram of the fully frustrated model.

At low temperature there are two phases a Fermi liquid metal characterized by a non zero density of states at zero energy and paramagnetic insulator with a gap in the one particle excitation spectra. The metallic solution disappears at the dotted line ending at U_{c2}, while the insulating solution persist down to the dotted line ending at U_{c1}. There is a region enclosed by the lines $U_{c1}(T)$ and $U_{c2}(T)$, where both the metallic and the insulating solutions are allowed. Within this region, there is a first order boundary where the two very different solutions cross in free energy, and several quantities experience a jump: the specific heat, the susceptibility, the number of doubly occupied sites, etc. The first order line has a negative slope indicating that the paramagnetic insulating phase has a higher entropy than the metallic phase. The line ends in an second order critical point, above it there is a smooth crossover between a metallic and an insulating regime.

At $T = 0$, we have shown [16] using ED that the metallic state is lower in energy than the paramagnetic insulator and therefore the first order line ends in a $T = 0$ second order quantum critical point (denoted U_{c2} in the figure) . The ED and QMC method confirmed that the qualitative phase diagram obtained from 2OPT is correct, with only the values of U_{c1} and U_{c2} slightly reduced. With ED we obtained $U_{c1} \approx 2.15$ and $U_{c2} \approx 3.05$. For comparison notice that the Hubbard III approximation gives $U_c = 1.73$, and the Brinkman-Rice approach which starts from the $U = 0$ limit gives $U_c \approx 3.3$. The metallic solution is characterized by a narrow quasiparticle peak at the Fermi energy with a width e_F^* that goes to zero as $U_c - U$; plus two high energy incoherent features at $\pm\frac{U}{2}$.

The magnetic phases of the models are displayed in figure 2. On bipartite (non frustrated) lattices the magnetic ordering preempts the Mott transition. We demonstrate this by calculating the Neel temperature of the Bethe lattice (dotted line). In this case we notice a continuous vanishing of the staggered magnetization that defines the Neel ordering temperature line. Therefore, the transition into an insulating state is due to a magnetic instability, realizing Slater's ideas.

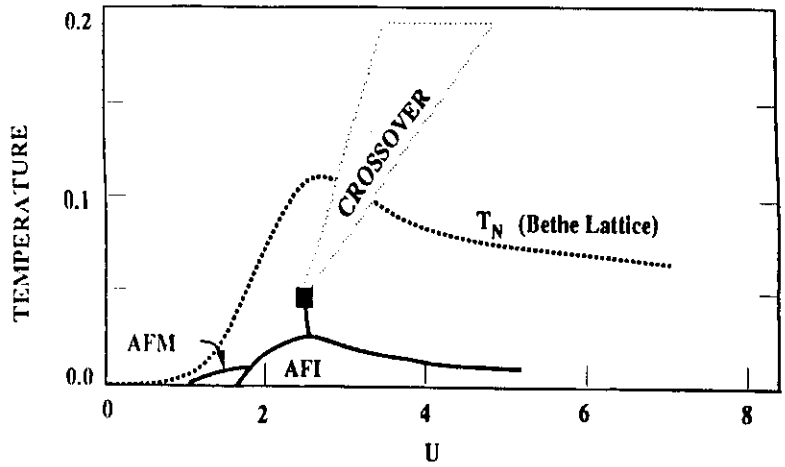

FIG. 2. Phase diagram with magnetic phases of the models discussed in the text.

As the degree of frustration is increased, the Neel line goes down in temperature. In particular for parameters $t_1^2 = 0.75t^2, t_2^2 = 0.25t^2$, it falls beneath the 2^{nd} order critical point and the first order transition becomes relevant, realizing Mott's scenario. Therefore we find that in a partially frustrated model (TSFF), the phase diagram features both a paramagnetic metal insulator transition at intermediate temperatures, and a Neel ordered phase at low temperatures. Also, for certain band structures, a small metallic antiferromagnetic phase is obtained.
To gain further insight on the nature of the transition, we investigated the behavior of various quantities as a function of U. We first plot in figure 3 the double occupation $< D >$ as a function of U as obtained from the different methods.

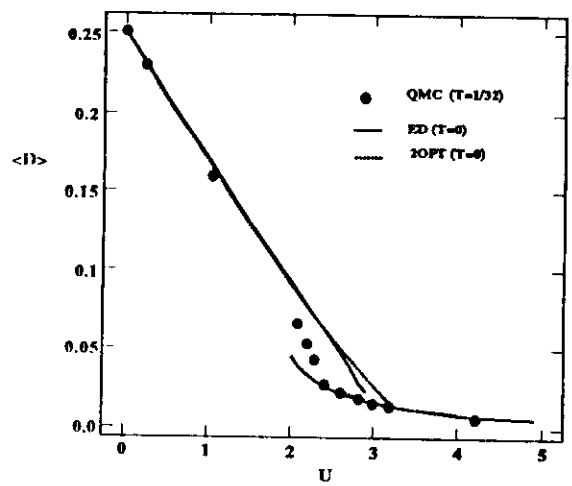

FIG. 3. Double occupation as a function of the interaction U.

There are two branches, corresponding to the metallic and insulating solutions at $T = 0$, which merge at $U_c \approx 3$. They show the excellent agreement of the exact diagonalization algorithm and the 2OPT in all parameter range, except very close to the MIT point at U_c. The QMC data being at an inverse temperature $\beta = 32$, shows that the effect of the temperature is to reduce the double occupation on the metallic side. In the insulating side, the effect is negligible since in this case there are no small energy scales. At this temperature the coexistence region is very small, and the data shows a jump in $< D >$ at $U \approx 2.4$. Notice that this result indicates that the Brinkman-Rice approach captures the singular part of $< D >$, but in addition we observe that this quantity does not vanish at the transition due to an additive non-singular part. We can thus parametrize $< D >= 0.235(\frac{U_c - U}{U_c}) + 0.015$ Also note that the magnetic moment is obtained from the double occupation through the identity $< m_Z^2 >= 1 - 2 < D >$. Therefore, we find that the magnetic moment is not saturated at the transition.
We also compare the value for the quasiparticle residue Z (inverse mass enhancement) as a function of U from the exact diagonalization method and the 2OPT (figure 4). For a small value of U the latter becomes exact, at an intermediate range they coincide and as the critical point is approached the

exact diagonalization method, that treats the interaction non-perturbatively, becomes more accurate. Using the projective self consistent method we obtained $U_c \approx 3.05$. Notice that the $Zvs.U$ line extrapolates towards that value. It is noticeable that a straight line from U_c can be obtained for a big range of the interaction. The mass renormalization in the limit of infinite dimensionality is identical to the quasiparticle weight. The critical behavior of the renormalized mass is thus $\frac{m*}{m} = Z^{-1} \approx 0.91(1-(\frac{U}{U_C}))^{-1}$ in agreement with the Brinkman-Rice picture. We can define then the useful scale $e_F^* = ZD$ that describes the width of the quasiparticle peak at the Fermi energy in the metallic phase.

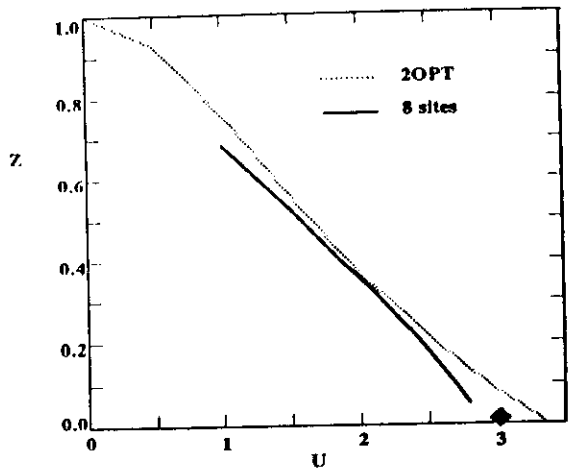

FIG. 4. The quasiparticle weight Z as a function of the interaction U.

In figure 5 we plot the inverse magnetic susceptibility $\chi_S^{-1} vs.U$ as obtained from the slope of the $< m_Z > vs.h$ curves calculated by QMC simulations at an inverse temperature $\beta = 16$. This quantity is given in units such that $\mu_B = 1$. Unlike the Brinkman-Rice approach this quantity remains finite at the transition due to to the existence of a non-zero superexchange constant $J = \frac{2t^2}{U} = \frac{D^2}{2U}$ in the uniform response. The numerical result can be parametrized according to an analytic expression [12]. We find $\chi^{-1} \approx 0.23(U_c - U)$ for the metallic phase, and $\chi^{-1} \approx J$ in the insulator phase (J is plotted for comparison).

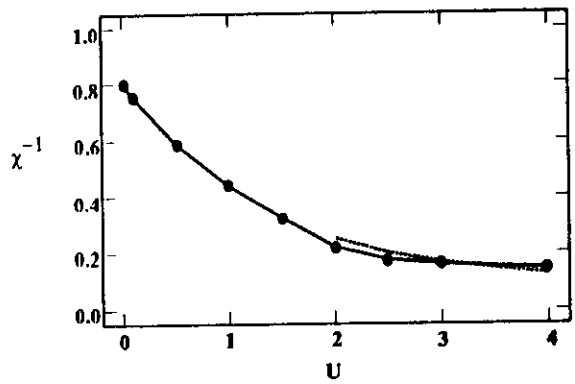

FIG. 5. Inverse of magnetic susceptibility at q = 0 (solid dots) and the magnetic exchange J (dashed line) as a function of the interaction U.

We also obtained the Wilson ratio as a function of interaction U. This quantity is displayed in figure 6 and is derived from figures 4 and 5. It is found to vanish at the critical point since while the specific heat diverges as $\frac{1}{e_F^*}$, the magnetic susceptibility is cut-off by $min\{T^{-1}, J^{-1} = 2U/D^2\}$.
Finally, in figure 7 we plot the value of the Hubbard gap as a function of U in both the paramagnetic and antiferromagnetic phase. As a definition for the magnitude of the gap we take twice the energy of the lowest energy pole of the Green function obtained from the exact diagonalization method. We show data extrapolated for finite size effects from systems of 3,5 and 7 sites. A $1/N_{sites}$ scaling behaviour is assumed. The results indicate that, following the insulating solution, the paramagnetic gap closes at a value $U_{c1} \approx 2.15$.

4. The Mott Transition as a function of doping

It is interesting to investigate the Mott transition as a function of doping in the Hubbard model. We believe that away from half filling and in the paramagnetic phase there is only one solution, and then we can investigate the behavior of various quantities as a function of filling factor.

We first show in figure 8, the particle occupation as a function of the chemical potential as obtained from QMC at $\beta = 16$. We note that the slope of the curve, i.e. the compressibility goes to zero at $\mu = 0$ as U_c is approached. For bigger values of U, we have a vanishing compressibility characteristic of an insulating state. It displays a gap equal to $U - 2D$ which compares very well with the results for the size of the gap from the exact diagonalization method (figure 7). Notice that for $U > U_c$ the $\delta vs.\mu$ curves approach half filling ($\delta = 0$) with a finite slope.

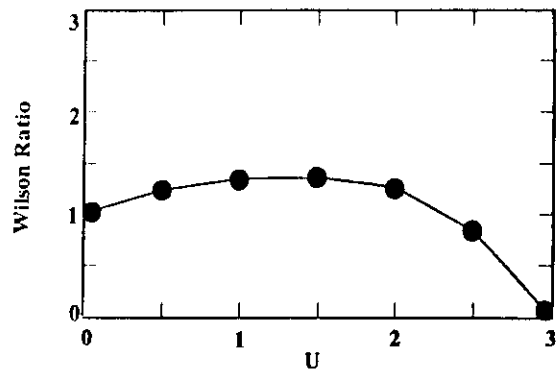

FIG. 6. Wilson ratio as function of the interaction U.

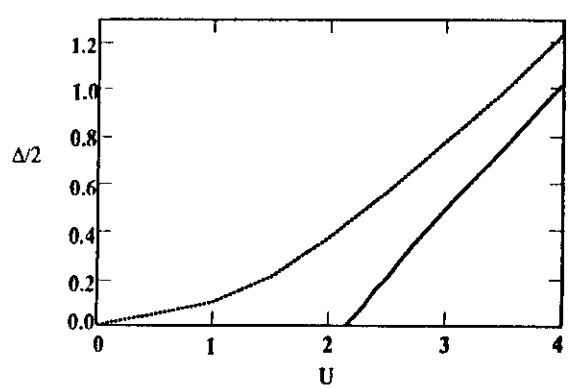

FIG. 7. Antiferromagnetic (dotted line) and paramagnetic (solid line) gap as function of the interaction U.

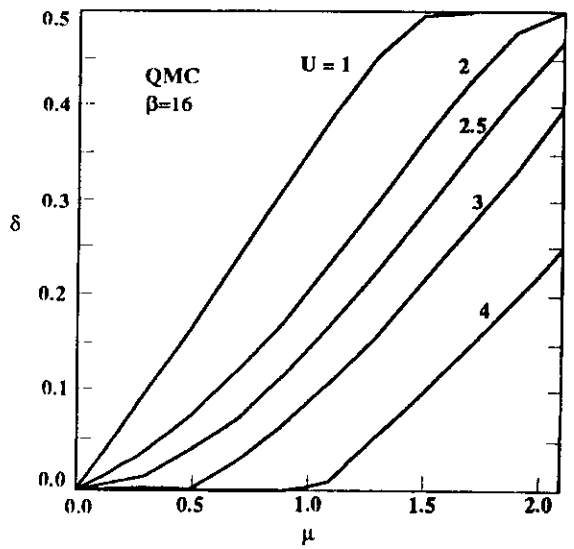

FIG. 8. Particle number versus the chemical potential for different values of the interaction U.

We also calculated the specific heat and spin suceptibility as a function of doping for the case $U = 3$. This places the system close to the Mott point, as it seems to be the case for compounds as $La_xSr_{1-x}TiO_3$ and the high T_C cuprates. These quantities are displayed in figure 9 and are obtained from QMC at $\beta = 32$. This compares rather well with the experiments of Tokura *et al.* on $La_xSr_{1-x}TiO_3$ [18]. The specific heat is consistent with the parametrization $\gamma \approx 0.28\delta^{-1}$, in units of $\frac{\pi^2 k_B^2}{3}\rho^0$, with $\rho^0 = \frac{4}{\pi D}$. The spin suceptibility is expressed in units of $\frac{\mu_B^2}{D}$

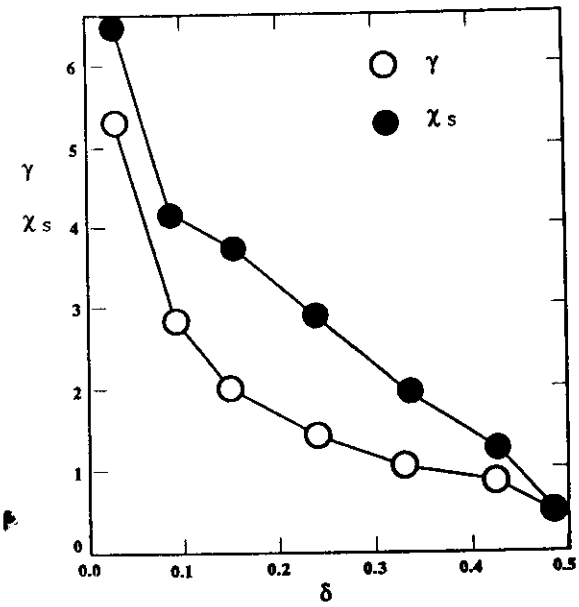

FIG. 9. Specific heat and spin suceptibility as function of doping for $U = 3$.

The Wilson ratio $(\chi_S/\gamma)/(\chi_S^0/\gamma^0)$ as function of doping is derived from these quantities (figure 10). Notice that its value is consistently lower than the experimental value $R = 2$. Whether this is due to a shortcoming of the mean field theory or it is some interesting effect of the many orbital character of the experimental system is an open problem.

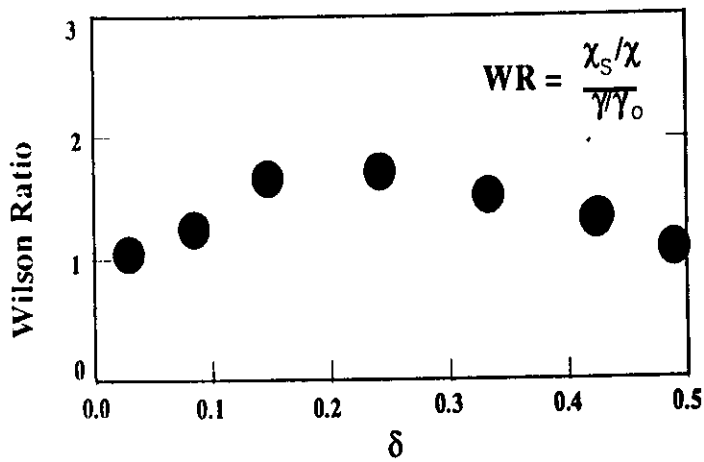

FIG. 10. The Wilson ratio as function of doping for $U = 3$.

The optical conductivity of a correlated electron system at $T = 0$ can be parametrized by

$$\sigma(\omega) = \frac{\omega_P^{*2}}{4\pi}\delta(\omega) + \sigma_{reg}(\omega) \tag{8}$$

where the coefficient in front of the δ-function is the Drude weight and ω_p^* is the renormalized plasma frequency. In the presence of disorder $\delta(\omega)$ is replaced by a lorentzian of width Γ.
The kinetic energy is related to the conductivity by the sum rule

$$\int_0^\infty \sigma(\omega)d\omega = -\frac{\pi e^2}{2\hbar^2 a} < T >= \frac{\omega_P^2}{4\pi} \tag{9}$$

where e is the electron charge and a the lattice constant. This expression is valid in any dimension. The Drude part can be directly obtained in terms of the quasiparticle weight in the limit of $d \to \infty$. It can be shown that $\frac{\omega_P^{*2}}{4\pi} = \frac{2e^2}{3\hbar^2 a} DZ$.
In figure 11 we plot the kinetic energy $< T >$ as a function of the doping ($\delta = 0$ at half filling, $\delta = 1/2$ at full filling), as obtained from QMC at $\beta = 16$.

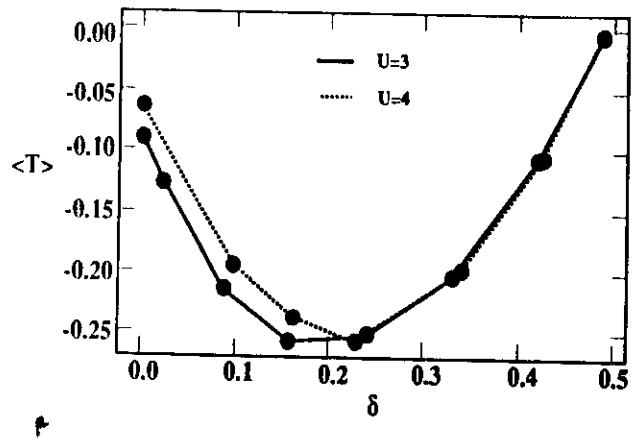

FIG. 11. The kinetic energy as function of doping.

In figure 12 we plot the kinetic energy $< T >$ as a function of the interaction U. This quantity is calculated at half filling in the paramagnetic metal and insulator phase, and also in the antiferromagnetic phase.

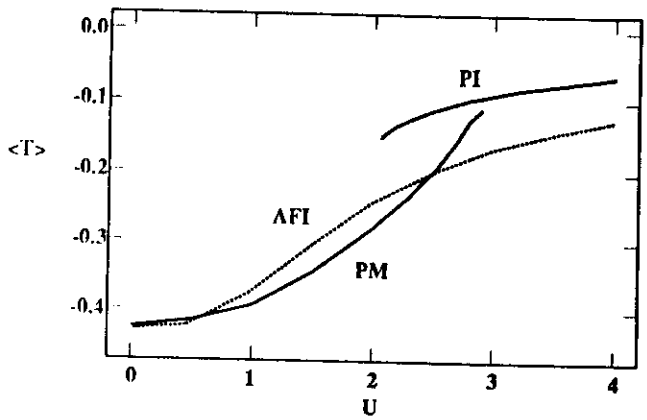

FIG. 12. Kinetic energy in the paramagnetic (metal and insulator) and antiferromagnetic (insulator) phase as a function of the interaction U. Obtained from the ED method.

Therefore, the quantities $< T >$ and Z, that are easily obtained within the present scheme, can be utilized to assess the validity of a simple one band Hubbard model to describe the low energy part of the optical conductivity of metal oxides.

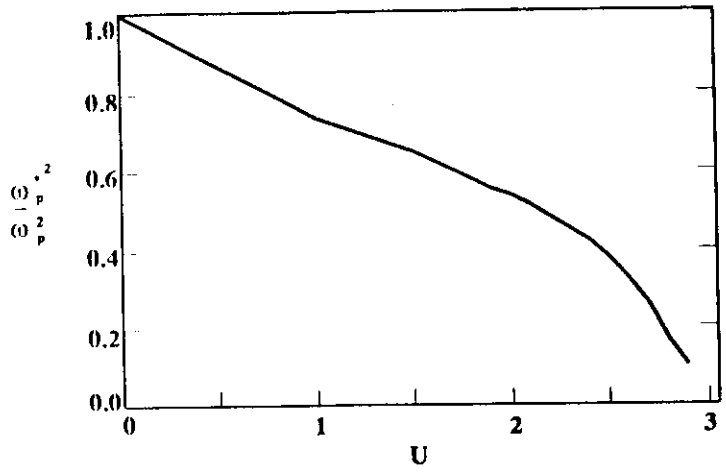

FIG. 13. Ratio of the Drude part to the total spectral weight as a function of the interaction U.

5. Conclusions

The solution of the Hubbard model in the limit of large dimensions has provided a framework where various early ideas can be reconciled and put in perspective.

One issue is whether a metal insulator transition can take place in the absence of magnetic order. The phase diagram presented in figures 1 and 2 answers this question in the affirmative for a frustrated lattice. The phase diagram has the same topology and even the same temperature scale as the experimentally observed phase diagram of V_2O_3 if we take a bare half-bandwidth of $1eV$ [17].

On the other hand, the investigation of the Mott transition as a function of doping allows to account for the critical behavior of various physical quantities observed in recent experiments in the $La_xSr_{1-x}TiO_3$ system [18]. We have further indicated, how the question of the optical conductivity of metal oxides can be approached within this framework.

The mean field methods developed here can be combined with more realistic density functional calculations of the bare band structure to provide a successful *ab initio* approach to the calculation of the physical properties of transition metal oxides. The density functional method captures the momentum dependence of the one particle self-energy while the mean field approach accurately incorporates the frequency dependence.

Acknowledgements: The results presented here have been worked out in collaboration with X.Y. Zhang and G. Moeller whose pleasant collaboration we gratefully acknowledge. We would also like to thank V. Dobrosavlevic, Q. Si and A. Georges for numerous valuable discussions. This work has been supported by the NSF DMR 92-4000.

---

[1] N. F. Mott, *Phil. Mag.* **6**, 287 (1961).
[2] W. Metzner and D. Vollhardt *Phys. Rev. Lett.* **62**, 324 (1989).
[3] A. Georges and G. Kotliar, *Phys. Rev. B* **45**, 6479 (1992).
[4] V. Janis, *Z. Phys. B* **83**, 227 (1991)
[5] V. Janis and D. Vollhardt, *Int. Journ. Mod. Phys. B*, Vol. 6, Nos 5 & 6, 731 (1992).
[6] A. Georges, G. Kotliar and Q. Si *Int. J. Mod. Phys. B* **6**, 705 (1992).
[7] M. Jarrell, *Phys. Rev. Lett.* **69**, 168 (1992).
[8] M. Rozenberg, X. Y. Zhang and G. Kotliar, *Phys. Rev. Lett.* **69**, 1236 (1992).
[9] A. Georges and W. Krauth, *Phys. Rev. Lett.* **69**, 1240 (1992).
[10] X. Y. Zhang, M. J. Rozenberg and G. Kotliar, *Phys. Rev. Lett.* **70**, 1666 (1993).
[11] A. Georges and W. Krauth, *Phys. Rev. B* **48**, 7167 (1993).
[12] M. J. Rozenberg, G. Kotliar and X. Y. Zhang *Phys. Rev. B* (April 1994).
[13] M. J. Rozenberg, G. Moeller and G. Kotliar (preprint)
[14] M. Caffarel and W. Krauth (preprint)
[15] G. Moeller, Q. Si, G. Kotliar and M. Rozenberg (preprint)
[16] M. J. Rozenberg, G. Moeller, and G. Kotliar, *SISSA #cond – mat/9402056*

[17] H. Kuwamoto, J. M. Honig, and J. Appel *Phys. Rev. B* **22**, 2626 (1980).
[18] Y. Tokura, Y. Taguchi, Y. Okada , Y. Fujishima and T. Arima, K. Kumagai, Y. Iye *Phys. Rev. Letts.* **70**, 2126 (1993).

Mott-Hubbard transition in infinite dimensions. II

M. J. Rozenberg, G. Kotliar, and X. Y. Zhang
Serin Physics Laboratory, Rutgers University, Piscataway, New Jersey 08854
(Received 19 July 1993; revised manuscript received 1 October 1993)

We discuss the Mott-Hubbard transition in light of the Hubbard model in infinite dimensions with special emphasis on the finite-temperature aspects of the problem. We demonstrate that the Mott transition at finite temperatures has a first-order character. We determine the region where metallic and insulating solutions coexist using second-order perturbation theory and we draw the phase diagram of the Hubbard model at half filling with a semicircular density of states. We discuss the lessons learned from the present treatment of the Hubbard model and the connection to other approximation schemes and to experiments on transition-metal oxides.

I. INTRODUCTION

The Mott transition, which is the metal-insulator transition induced by the electron-electron interactions in a periodic system, has been investigated theoretically and experimentally for many years.[1] Experimentally it seems to be realized in three-dimensional transition-metal oxides such as V_2O_3 and can be driven by varying the pressure, the temperature, and the composition.

From a theoretical point of view, several ideas have been put forward. Hubbard first introduced the notion of Hubbard bands, which are formed by the states describing propagating empty and doubly occupied sites. For large U these bands split, and as U is reduced there is a critical value of U where the two bands merge again.[2] This is the Hubbard picture of the metal-insulating transition.

Brinkman and Rice,[3] building on the work of Gutzwiller, started from the metallic phase which they described as a strongly renormalized Fermi liquid with a characteristic Fermi energy scale gradually collapsing as the transition is approached. The metal-insulator transition in this view is driven by the disappearance of the Fermi liquid quasiparticles. Slater[4] pointed out that the metal-insulator transition is always accompanied by long-range antiferromagnetic order, and viewed the doubling of the unit cell, which makes the band structure of the system that of a band insulator, as the driving force behind the metal-insulator transition.

Building on earlier ideas,[5-9] a mean-field theory of strongly correlated electron systems has been developed. It is based on a mapping of the models of strongly correlated electrons onto impurity models supplemented by a self-consistent condition.[10,11] This approach becomes exact in the limit of infinite dimensions[5] and can be investigated using a variety of techniques. In this paper, we complete our study of the Mott transition in the Hubbard model in large dimension, expanding on our previous publications.[12,13] In particular, we make comparisons of our solutions to experimental observations, and find good agreement considering the relative simplicity of the model. Related work on this problem has been carried out independently by other groups.[14-17]

The paper is organized as follows: In Sec. II, we start by briefly reviewing the general framework of Ref. 11 to present the set of self-consistent equations that describe the Hubbard model in infinite dimensions. We concentrate on the semicircular density of states which can be realized on a Bethe lattice, or other lattices having various amounts of magnetic frustration. The mean-field equations are functional equations that determine a Weiss field function G_0 and involve a self-energy functional of an Anderson impurity model $\Sigma_{imp}[G_0]$. Two realizations of the Hubbard model which share the same density of states but have very different magnetic properties are introduced later to shed light on the issue of magnetic ordering. We close the section with a discussion of the methods used to analyze this problem.

To study the mean-field equations we use a combination of exact methods such as quantum Monte Carlo (QMC) and analytic arguments exploiting the well-understood structure of the Anderson impurity model. We also rely on an approximate method which was proposed by Georges and Kotliar to extract low-temperature information. We stress that, while at high temperature this method[13] gives results in very good agreement with the quantum Monte Carlo, in principle is only an approximate scheme and we point out some of its limitations. The results obtained with this method are useful because they provide a concrete analytic realization of the functional $\Sigma_{imp}[G_0]$ defined in Sec. II, and illustrate in a simple example the important role played by the self-consistency condition.[9]

In Sec. III we describe the thermodynamics and present the finite-temperature phase diagram of the system. We study the dependence of the phase diagram on the degree of magnetic frustration. In frustrated lattices the phase diagram features a region bounded by two values of the interaction U_{c1} and U_{c2}, where a metallic and an insulating phase coexist. The actual transition takes place at an intermediate value U_c where the free energies of the two solutions cross. We demonstrate that, at finite T, $U_{c1} < U_c < U_{c2}$, and the metal-insulator transition is of the first order, like a liquid-gas transition. While the region of stability of the two phases is model dependent and will vary upon changing the den-

0163-1829/94/49(15)/10181(13)/$06.00

sity of states or adding more general interactions to the Hamiltonian, there are some general lessons that can be drawn by studying the disappearance of the metallic and the insulating solution. These are general scenarios for describing a strongly correlated metal and a Mott insulator.

In Sec. IV we discuss the destruction of the metallic solution. It has many features in common with the Brinkman-Rice scenario for the disappearance of the metal and is realized near a critical value of the interaction U_{c2}.

In Sec. V we analyze the disappearance of the insulating solution. We show that there is another critical point U_{c1} below which the insulating solution disappears. The existence of this point is related to Hubbard's early ideas.

Section VI is devoted to the study of the correlation functions. In particular, we address the question of how they behave as the transition takes place. We rely on a combination of analytical arguments and QMC simulations to discuss these points.

In Sec. VII, we make qualitative comparisons to existing experimental data, in V_2O_3[18] and in $La_{1-x}Sr_xTiO_3$.[19] The agreement leads us to believe that the Hubbard model and its extended version are at least qualitatively correct models for describing these systems. We conclude with some theoretical questions raised by our work.

II. THE SELF-CONSISTENT EQUATIONS

We briefly review the self-consistent equations which give the paramagnetic solution in large d, following the scheme of Ref. 9. The central object in this approach is a quantity G_0 which plays the role of the effective field in magnetic systems. G_0 is defined in an effective local action S obtained by integrating out all the degrees of freedom except for a single site 0,

$$S[G_{0\sigma}] = -\int\int d\tau d\tau' c_\sigma^\dagger G_{0\sigma}^{-1} c_\sigma + \int d\tau U(n_\uparrow - \tfrac{1}{2})(n_\downarrow - \tfrac{1}{2}). \quad (1)$$

This action is identical to that of an Anderson impurity model with arbitrary hybridization. The self-consistent equations for the Weiss field G_0 are written in terms of an impurity self-energy $\Sigma_{\rm imp}(G_0) = \langle c^\dagger c\rangle^{-1}_{S(G_0)} + G_0^{-1}$ and the lattice density of states $\rho(\epsilon) = \sum_k \delta(\epsilon_k - \epsilon)$,

$$[G_0^{-1} - \Sigma_{\rm imp}(G_0)]^{-1} = \int \frac{\rho(\epsilon)d\epsilon}{i\omega - \epsilon - \Sigma_{\rm imp}(G_0)}. \quad (2)$$

The impurity self-energy evaluated at the self-consistent G_0 gives the self-energy of the Hubbard model in infinite dimensions.[9]

We use a semicircular density of states, $\rho(\epsilon) = \frac{2}{\pi D}\sqrt{1-(\frac{\epsilon}{D})^2}$. The set of self-consistent equations then becomes:

$$G_0^{-1} = i\omega_n - t^2 G(i\omega_n), \quad G = -\langle c^\dagger c\rangle_{S(G_0)} \quad (3)$$

$G(i\omega_n)$ being the *local* Green's function of the Hubbard model. The spin index has been removed. This density of states is realized in the Bethe lattice with coordination d, in the limit that d becomes infinite, and with Hubbard's hopping parameter equal to $\frac{t}{\sqrt{d}}$. In this case $t = D/2$. This lattice with nearest-neighbor hopping, if not frustrated, will strongly favor a Néel-ordered state at low temperatures.

The semicircular density of states is also realized in the fully frustrated model,[12,20]

$$H_{\rm FF} = -t\sum_{i,j=1,d}\epsilon_{ij}c_{i\sigma}^\dagger c_{j\sigma} + U\sum_i n_{i\uparrow}n_{i\downarrow}. \quad (4)$$

Summation over repeated spin indices is assumed. Here ϵ_{ij} are quenched, independently distributed, Gaussian random variables with zero mean and a variance $\langle\epsilon_{ij}^2\rangle = \frac{1}{d}$. This model has a semicircular density of states with a bandwidth equal to $2t$ and therefore shares the same *local* properties as the Bethe lattice, but of course is not expected to display Néel order at any finite temperature. Finally we can vary the degree of frustration by studying a two-sublattice version of the fully frustrated model (TSFFM). The Hamiltonian is given by:

$$H_{\rm TSFFM} = -t_1\sum_{i,j\in A\text{ or }B}\epsilon_{ij}c_{i\sigma}^\dagger c_{j\sigma} - t_2\sum_{i\in A\, j\in B}\epsilon_{ij}c_{i\sigma}^\dagger c_{j\sigma} + U\sum_{i\in A\cup B} n_{i\uparrow}n_{i\downarrow}. \quad (5)$$

This model interpolates between the fully frustrated lattice and the Bethe lattice in the antiferromagnetic phase while still sharing a semicircular local density of states. In this case $D = \frac{\sqrt{t_1^2+t_2^2}}{2}$. Notice that while the Hamiltonians (4) and (5) contain randomness, the single-particle properties are self-averaging. The single-particle Green's functions are the same for any typical realization of the random variables ϵ_{ij}.

As in our previous publications, we have studied the semicircular density of states instead of the Gaussian density of states which is realized in the large-dimension limit of a hypercubic lattice, because the latter has long tails which prevent the development of a true Hubbard gap. For a study of the hypercubic lattice see Refs. 14 and 15.

When antiferromagnetism sets in, the Weiss field depends on the sublattice and the spin. For a general bipartite lattice in the Néel phase $G_{A\sigma} = G_{B-\sigma}$ the equations were derived in Ref. 11. For the Bethe lattice, the equations are simplified to:

$$G_{0A\sigma}^{-1} = i\omega - t^2 G_{B\sigma}, \quad (6)$$

$$G_{0B\sigma}^{-1} = i\omega - t^2 G_{A\sigma}, \quad (7)$$

where A denotes one sublattice and B the other. The two impurity Green's functions G_A and G_B are evaluated independently, given $G_{0A\sigma}$ and $G_{0B\sigma}$ and the single-site action S defined at the beginning of this section.

Finally, in the two-sublattice fully frustrated model, which mimics an intermediate degree of frustration, the

mean-field equations in a phase where the A and B sublattices magnetize in opposite directions are given by

$$G^{-1}_{0A\sigma} = i\omega - t_1^2 G_{A\sigma} - t_2^2 G_{B\sigma}, \tag{8}$$

$$G^{-1}_{0B\sigma} = i\omega - t_1^2 G_{B\sigma} - t_2^2 G_{A\sigma}. \tag{9}$$

In a previous work[13] we have discussed the fact that the exact treatment of the problem by a quantum Monte Carlo solution of the impurity can be reproduced, remarkably well, by the second-order perturbative calculation proposed in Ref. 21. The perturbative calculation allows us to investigate the low-temperature behavior of the system, including $T = 0$, which is unattainable by the QMC approach. To second order in perturbation,

$$\Sigma[G_0](\tau) = -U^2 G_0^3(\tau). \tag{10}$$

We can understand the success of this approximation for the following reasons. (1) It is good for weak couplings ($U \ll t$) by construction, since the expansion is around $U = 0$. As shown by Yamada and Yosida (YY),[21] it is able to produce not only the Abrikosov-Suhl resonance, but also the upper and lower incoherent bands as well. YY showed that the fourth-order correction is two orders of magnitude smaller than the second-order contribution for the range of the interaction where the metal-insulator transition occurs. (2) The atomic limit is exactly captured. When U is very large, and the system is deep in the insulating side, $G_0^{-1} \approx i\omega_n$, the nonmagnetic Hartree-Fock solution of the Green's function becomes exact,

$$G_L(i\omega) = \frac{1/2}{G_0^{-1}(i\omega_n) - U/2} + \frac{1/2}{G_0^{-1}(i\omega_n) + U/2}, \tag{11}$$

and therefore the self-energy reads,

$$\Sigma = \left(\frac{U}{2}\right)^2 G_0(i\omega_n), \tag{12}$$

which is identical to the self-energy that results from inserting G_0 in Eq. (10) and Fourier transforming. Thus, the second-order approximation is at least an interpolation scheme which becomes exact for both the $U \to 0$ and $U \to \infty$ limits.

III. PHASE DIAGRAM AND THERMODYNAMICS

As discussed in previous publications, the system of Eqs. (1), (2), and (3) has two types of solutions, metallic when $G(0) = \frac{2}{iD}$ and insulating when $G(0) = 0$. This distinction is precise at zero temperature. At finite but small temperatures, a sharp distinction between a metallic and an insulating solution can still be made, since we find a region where *two* solutions are allowed. One can be continuously connected to the $T = 0$ metallic solution, and displays a peaklike feature at the Fermi energy. The other solution can be connected to the $T = 0$ insulating solution, and the Green's function extrapolates to zero at zero frequency. As the temperature is further increased this region of coexistent solutions disappears and we are left with a rapid crossover from a metalliclike solution to an insulating one. This is possible because at finite temperature there is no qualitative distinction between a metallic and an insulating shape.

As mentioned in the introduction, at low temperatures there are two critical values U_{c1} (the smallest U that allows an insulating solution) and U_{c2} (the largest U permitting a metallic solution) between which the mean-field equations have two solutions. To determine the phase diagram we proceed in three steps: (a) We first determine the region where the two paramagnetic solutions coexist. (b) We then compare their free energy, crossing of which determines the phase boundary. (c) We finally study the magnetically ordered phase and calculate the Néel temperature to check whether the metal-insulator transition found in step (b) is preempted by a magnetic ordering transition.

We use the second-order perturbation theory scheme throughout most of this work because the low temperature prevents the extensive use of QMC. We checked however that the existence of two solutions is a genuine feature of the large-d Hubbard model and not an artifact of the second-order approximation by performing a few quantum Monte Carlo runs. In Fig. 1 we show a metallic and an insulating Green's function obtained for the same value of the parameters U=2.8 and T=1/64, as is obtained from both QMC and the perturbative calculation. Throughout the paper the bandwidth D is taken to be unity. To select an insulating or a metallic solution we choose G_0 obeying $G_0(i\omega) = \frac{1}{i\omega}$ or $G_0(0) \neq 0$ respectively as the initial guess in the substitution procedure for solving the mean-field equations.

The energy is computed from the Green's function by

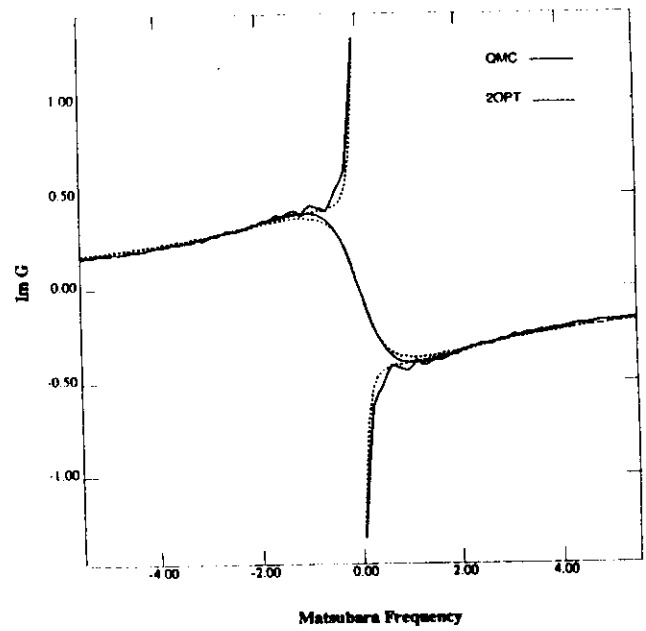

FIG. 1. Comparison of the insulating and metallic Green's function obtained using the quantum Monte Carlo algorithm and the perturbative calculation. The value of the interaction $U = 2.8$ and the inverse temperature $\beta = 64$.

$$E = T\frac{1}{2}\sum_{nk}(i\omega_n + \epsilon_k)G_k(i\omega_n). \tag{13}$$

The entropy is given by

$$S(T) = \int_0^T \frac{C_v}{T'}dT' + S(0), \tag{14}$$

where C_v is evaluated numerically by differentiating the energy. $S(0)$ is zero for the metallic side and ln(2) for the insulating side, reflecting the double degeneracy of the paramagnetic insulating phase.

The physical critical line where the first-order phase transition takes place is determined by equating the free energies of the two states,

$$F_M - F_I = E_M - E_I - (S_M - S_I)T. \tag{15}$$

To gain insights into the nature of the two coexistent solutions we plot the zero-temperature spectral function of the metallic and the insulating state in Fig. 2. The metallic state of the system can be well described by a narrow central quasiparticle peak characterized by an effective Fermi energy $\Delta \equiv zD$ where z is the quasiparticle weight, $z = (1 - \frac{d\Sigma}{d\omega})^{-1}$, plus two high-energy incoherent features at $\pm\frac{U}{2}$ corresponding to the upper and lower Hubbard bands. The quasiparticle weight z as a function of U is shown in Fig. 3. The insulator state consists of incoherent features only. Notice however that the shapes of the incoherent features of the metallic and the insulating phase are very different.

Figure 4 shows the calculated internal energy as a function of the temperature for two values of the interaction U. For the smaller value of U the temperature dependence of the internal energy of the metal displays a characteristic Fermi liquid T^2 behavior in the low-temperature region. The characteristic energy scale in this regime is set by the renormalized Fermi energy. At higher temperatures we see a thermal activation of the incoherent features. In the case of the insulator we observe only this last effect at an energy scale $U - 2D$.

In Fig. 5 we plot the specific heat C_v as a function

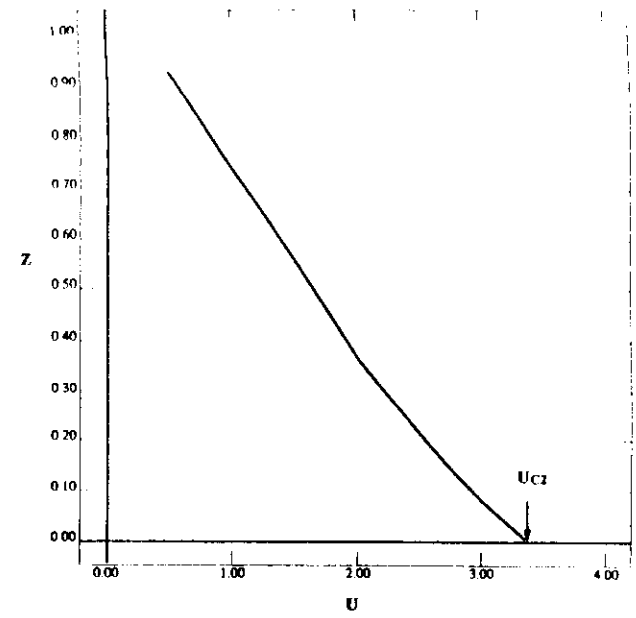

FIG. 3. Quasiparticle weight z as a function of interaction U, obtained with the $T = 0$ self-consistent perturbative calculation.

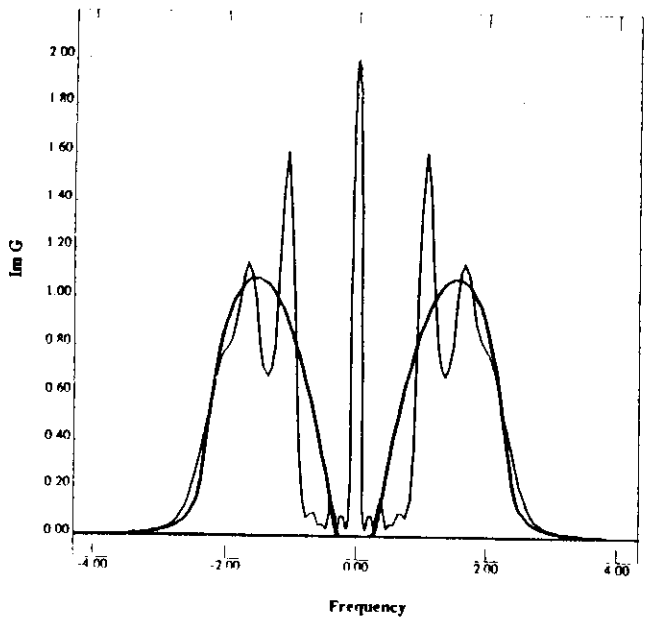

FIG. 2. Density of states for the metallic (thin line) and insulating (bold line) solutions at $T = 0$ and the same value of the interaction $U = 2.9$, obtained with the self-consistent perturbative calculation.

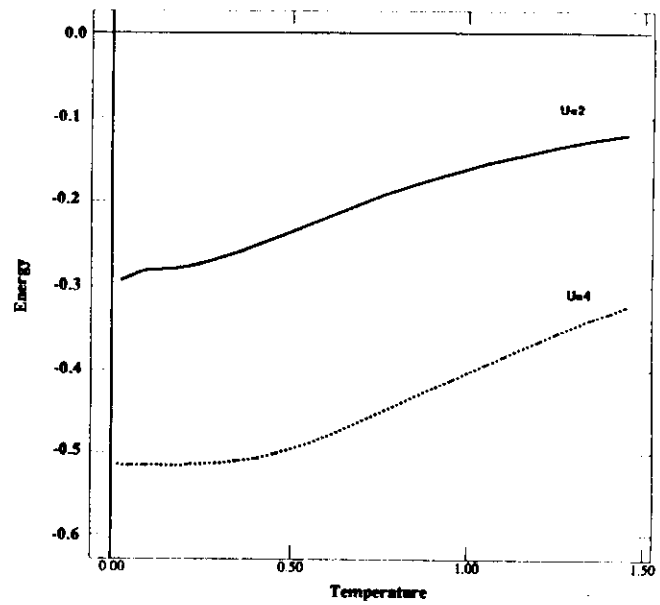

FIG. 4. Energy as a function of the temperature for a value of $U = 2$ in the metallic region (solid line), and $U = 4$ in the insulating phase (dotted line).

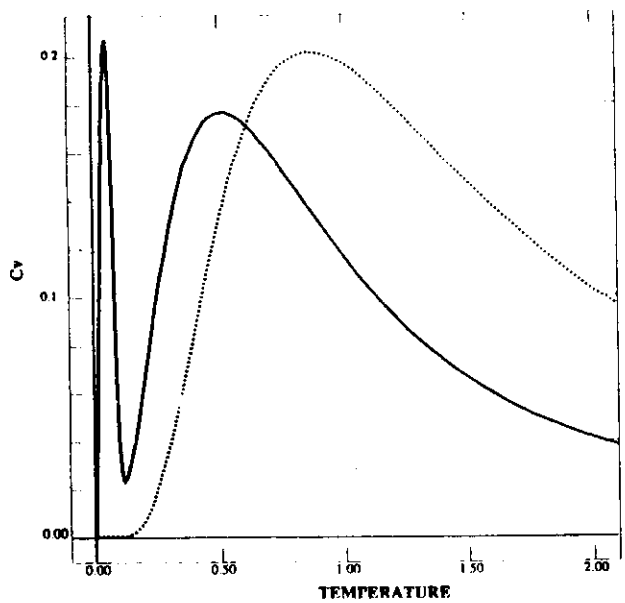

FIG. 5. Specific heat C_v as a function of temperature. The solid line is for $U = 2$ and the dashed line corresponds to $U = 4$. In the metallic case ($U = 2$) it is apparent the separation of energy scales. The linear part, at low T, ends at $T \sim \Delta$, and the thermal activation of the incoherent features peaks at the bigger scale $T \sim U - 2D$. This last effect is the only one present in the insulating case.

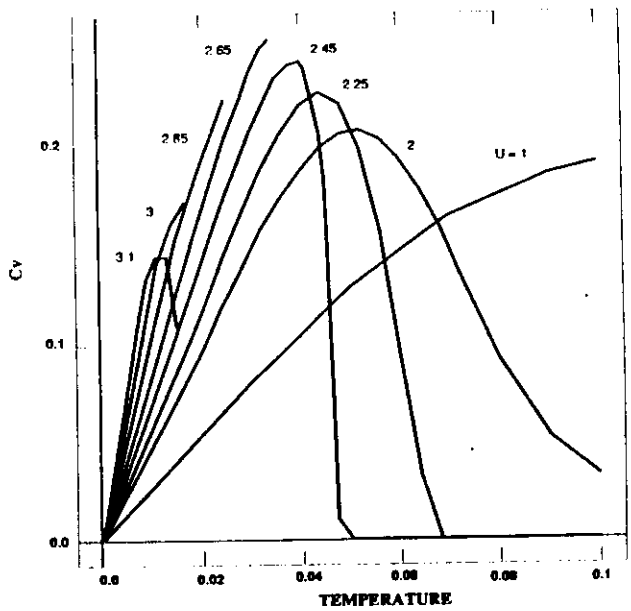

FIG. 6. Specific heat C_v as a function of temperature for several values of U.

of the temperature. The curves are obtained through numerical differentiation of $E(T)$. In the strongly correlated metallic phase we find a separation of scales since Δ is much smaller than $U - 2D$. At higher T a thermal activation peak appears at a scale $U - 2D$ in both the metallic and insulating cases. The linear-in-T Fermi liquid behavior is observed in the low-temperature region, with the slope γ proportional to $m^* \sim (U_{c2} - U)^{-1}$, as shown in Fig. 6

The integral (14) gives the entropy as a function of temperature. As expected the integral over the quasiparticle peak is equal to ln2 as shown in Fig. 7. As can be seen in Fig. 6, for larger values of U but with $U < U_{c2}$ the metallic solution disappears discontinuously before the entropy reaches ln2. Therefore, we define a coherence temperature T_* as the temperature where the entropy reaches the value of $\frac{\ln 2}{2}$. The physical relevance of T_* is that it delineates the temperature range where Fermi liquid theory is valid; see Fig. 8.

The comparison of the kinetic energy $T = \langle \sum_k \epsilon_k c_k^\dagger c_k \rangle = \sum_{nk} \epsilon_k G_k(i\omega_n)$ and the potential energy $V = U \sum \langle n_\uparrow n_\downarrow \rangle$ of the two solutions, is shown in Fig. 9 We find that the difference in the internal energy of the two states is much smaller than the corresponding difference in the kinetic and potential energy. The gain in kinetic energy by delocalization is almost perfectly canceled by the loss in potential energy due to the Coulomb repulsion in doubly occupied sites. This makes the higher-order corrections from higher-order terms in the Yamada-Yosida perturbation theory important for resolving the relative stability of the metallic and the insulating solution at *zero temperature*. We nevertheless expect the small energy difference between the two states to be a general feature of the problem and not an artifact of second-order perturbation theory. In fact the near degeneracy of the metallic and the insulating states near U_{c2} follows from the bifurcation of two stationary points of the free-energy functional at U_{c2}

We can take advantage of the numerical speed of the perturbative calculation to obtain a detailed phase diagram for the model defined by Eqs. (1), (2), and (3). The first-order phase boundary is determined by the crossing of the free energy of the two solutions. It ends in a crit-

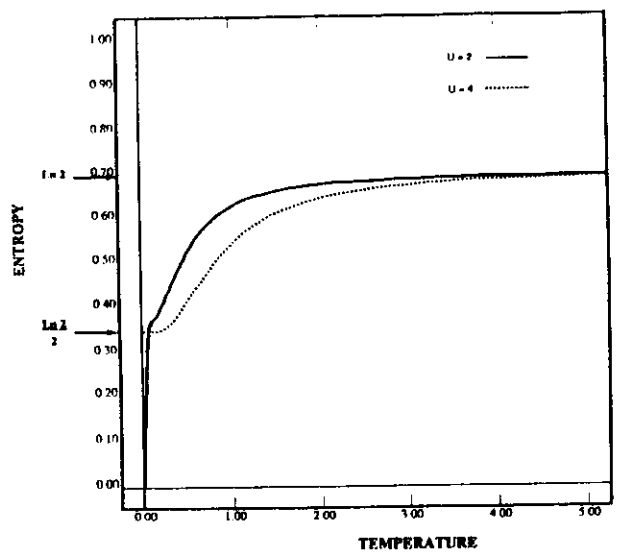

FIG. 7. Entropy per spin as a function of temperature for two different values of interaction, $U = 2, 4$.

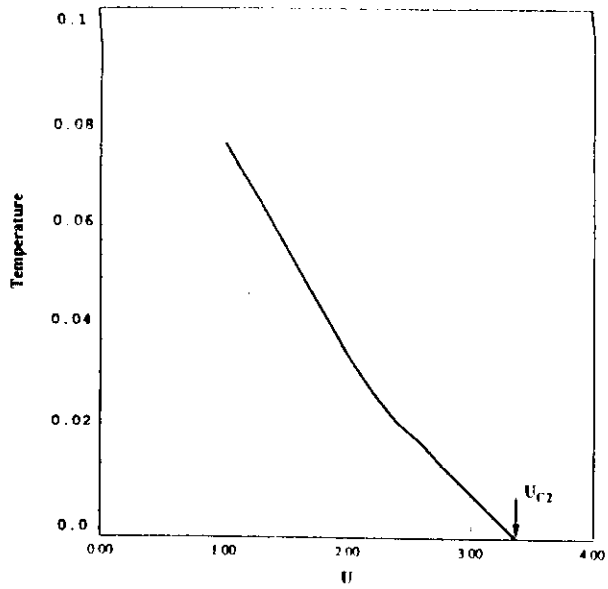

FIG. 8. Temperature value where the entropy reaches $\frac{\ln 2}{2}$ as a function of the distance to U_{c2}. This temperature defines the region where the Fermi liquid description is applicable.

ical point where a crossover region starts. This is displayed in Fig. 10. As emphasized before, due to the very small energy difference between the solutions, we expect the position of the phase boundary to be only approximately correct. We have observed in QMC runs that, for instance, the value of the U_{c1} line that denotes the disappearance of the insulating solution was shifted to a smaller value of the interaction U by an amount of order of $\sim 10\%$.

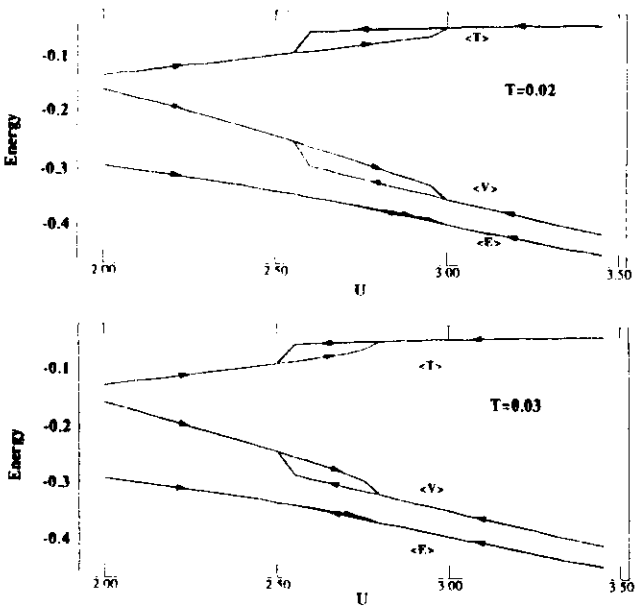

FIG. 9. The kinetic, potential, and internal energy as functions of U for (a) $T = 0.02$ and (b) $T = 0.03$. The hysteresis effect is clearly observed.

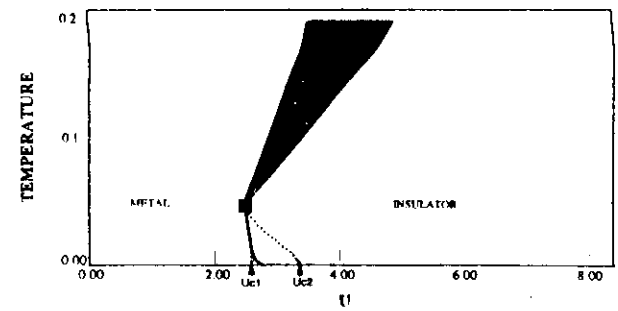

FIG. 10. Phase diagram of the fully frustrated Hubbard model at half filling. It is possible to move continuously from one phase to the other since at high T the transition becomes a crossover. The solid line is obtained by comparing the free energies of the two solutions in the region where they are both allowed. The dashed lines indicate the region where the metallic and the insulating solutions coexist. The filled square indicates the end of the first-order line in a second-order point.

We now turn to the determination of the Néel phase boundary. It depends on the nature of the lattice. For the Bethe lattice we solve Eqs. (6) and (7), while for the TSFFM introduced before, which mimics a finite degree of frustration, we solve Eqs. (8) and (9). The QMC method is used to estimate the magnetic phase boundary by solving the equations in the low-temperature region and determining the temperature where the staggered magnetization vanishes. The Néel temperature can be analytically determined on the insulating side for large U, and is given by $J_2 - J_1 = 2(t_2^2 - t_1^2)/U$. We mention in passing that the perturbative calculation does not correctly capture the magnetically ordered phase (see discussion in Sec. VI).

Figure 11 shows the phase boundary between paramagnetic states and antiferromagnetic states on the Bethe lattice. In this case, all the low-temperature features of the phase diagram discussed above are preempted by the onset of the antiferromagnetic state. On the other hand, for the case of the two-sublattice fully frustrated model, with values of $t_1^2 = \frac{1}{4}t^2$ and $t_2^2 = \frac{3}{4}t^2$, the Néel tempera-

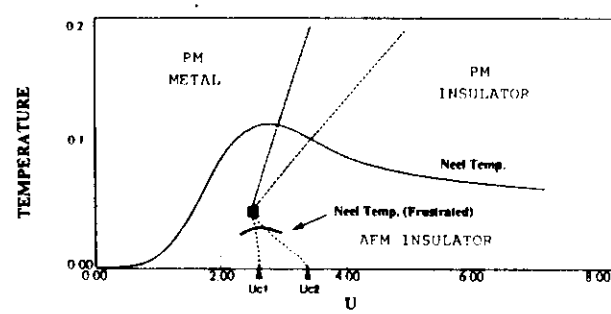

FIG. 11. Thin line corresponds the Néel temperature of the regular Bethe lattice as a function of interaction U. The bold line denotes an upper bound for the same quantity for the two-sublattice fully frustrated model with values $t_1^2 = 0.25t^2$, $t_2^2 = 0.75t^2$. The dotted lines are displayed for comparison to Fig. 10.

ture is much reduced. An upper bound for the $T_{\text{Néel}}$ as obtained from QMC simulations is indicated in Fig. 11. Simulations also indicate a jump in the Néel temperature line as the interaction U crosses the first-order transition boundary. The $T_{\text{Néel}}$ on the metallic side is smaller than the one on the insulating side.

It is clear that Slater's point of view is completely correct for nonfrustrated lattices such as the Bethe lattice with nearest-neighbor hopping only. The onset of antiferromagnetism makes the metal-insulator transition within the paramagnetic phase completely irrelevant. On the other hand, it is also clear that the presence of magnetic frustration makes Mott's viewpoint fully relevant, as demonstrated in the above diagram of the two-sublattice fully frustrated model.

IV. THE BREAKDOWN OF THE METALLIC SOLUTION

In this section we investigate the fate of the metallic solution. While we cannot settle the domain of stability of the metallic solution at zero temperature with the present approach, it is quite clear that the metal and the insulator are very close in energy and therefore the investigation of the metallic phase is of interest in the light of the considerably large mass renormalizations observed in some transition-metal oxides.

The destruction of the metallic state is driven by the collapse of the Fermi energy scale Δ which we showed is proportional to $U_{c2} - U$. From the mean-field equation $G_0^{-1} = i\omega_n - t^2 G$, we realize that this scale is also the *bandwidth* of the conduction-electron bath which hybridizes with the local impurity in the Anderson model picture. It is easy to understand, then, that for sufficiently large U this scale vanishes. Imagine solving the system of Eqs. (1), (2), and (3) by iteration. Consider a conduction-electron bandwidth Δ^n (W^n in the notation of Ref. 12) at the nth iteration step. For large U, solving the Kondo problem produces a bandwidth $\Delta^{n+1} = e^{-U/t}\Delta^n$. Therefore, the effective energy scale iterates to zero for $n \to \infty$.

Close to U_{c2}, there is a clear separation of energy scales and the local Green's function can be written as a sum of a low-energy and a high-energy part: G_l and G_h. The high-energy part resembles the solution of an atomic problem while the low-energy part obeys a scaling form.

In terms of a spectral representation:

$$G_l = \int_{-\infty}^{\infty} \frac{\rho_l(\epsilon)}{i\omega - \epsilon} d\epsilon \tag{16}$$

$$G_h = \int_{-\infty}^{\infty} \frac{\rho_h(\epsilon)}{i\omega - \epsilon} d\epsilon, \tag{17}$$

with $\rho_l(\epsilon) = \frac{1}{t} f(\frac{\epsilon}{\Delta})$ exhibiting a scaling form as $\Delta \propto U_{c2} - U$ goes to zero. $\rho_h(\epsilon)$ describes the high-energy nonscaling parts (Hubbard bands) centered around $\pm U/2$. A somewhat oversimplified but transparent picture of the spectral function is obtained by taking ρ_h to be two semicircles with overall weight $1 - \Delta/D$, $t = D/2$. The calculation of the scaling function f is an open problem, in the exact solution of the large-d Hubbard model. Here we determine it within the second-order perturbation theory scheme outlined in Sec. II.

Approaching the transition, G_0 develops a pole at a scale $\sqrt{\Delta t} \gg \Delta$. The pole can be determined exactly from the relation $G_0^{-1} = i\omega - t^2 G$. In the frequency range of $\Delta \ll \omega \ll U/2$, the Green's function can be simplified to

$$G = \frac{2}{\omega}\int_0^{\infty} \rho_l(\epsilon) d\epsilon - 2\omega \int_0^{\infty} \frac{\rho_h(\epsilon)}{\epsilon^2} d\epsilon + i\pi\rho(\omega), \tag{18}$$

where particle-hole symmetry $\rho(-\epsilon) = \rho(\epsilon)$ has been used to change the integration limit. In the energy region we are considering, the imaginary part is negligibly small and we will ignore it in the following calculations.

$$G_0^{-1} = (1 + 2t^2 C)\omega - \frac{2t^2 \Delta F}{\omega}, \tag{19}$$

where $F = \frac{1}{t}\int_0^{\infty} f(x)dx$ and $C = \int_0^{\infty} \frac{\rho_h(\epsilon)}{\epsilon^2} d\epsilon$. The pole results at $\omega_0 = \sqrt{\Delta}(\frac{2t^2 F}{1+2t^2 C})^{1/2}$.

Notice that the existence of this pole follows from the general scaling argument. Now, combining this with the second-order expression for the self-energy, one can make further progress and determine the value of U_{c2} analytically.

The self-energy is $\Sigma = -U^2 G_0^3(\tau)$, which can be conveniently expressed in terms of the density of states of the G_0,

$$\Sigma = -2\omega U^2 \int_0^{\infty}\int_0^{\infty}\int_0^{\infty} \frac{\rho_0(\epsilon_1)\rho_0(\epsilon_2)\rho_0(\epsilon_3) d\epsilon_1 d\epsilon_2 d\epsilon_3}{(\epsilon_1 + \epsilon_2 + \epsilon_3)^2 - \omega^2} \tag{20}$$

where $\rho_0(\omega) = -\frac{1}{\pi}\text{Im}G_0(\omega)$. As $\Delta \to 0$, ρ_0 develops a δ-like peak positioned at ω_0 with a weight of $\frac{1}{2(1+2t^2 C)}$. Therefore, the integrals can be performed in closed form,

$$\Sigma = -\frac{U^2\omega}{4(1 + 2t^2 C)^3(9\omega_0^2 - \omega^2)}, \tag{21}$$

as $\Delta \to 0$.

Comparing this expression with the one given by its definition, $\Sigma = G_0^{-1} - G^{-1} = -\frac{D\omega}{\Delta}$, where only the most singular term at small ω is kept, at $U = U_{c2}$ (i.e., $\Delta = 0$), we have

$$U_{c2} = 3D(1 + D^2/U_{c2}^2), \tag{22}$$

where $D = 2t$, and the approximations $F \approx \frac{1}{2D}$ and $C \approx \frac{2}{U_{c2}^2}$ that follow from the parametrization discussed before are used. The value at which the metallic solution disappears is then $U_{c2} = 3.28D$ which is very close to the numerically determined value $U_{c2}^{\text{num}} = 3.37D$. From Eq. (21) it is clear that the scaling part of Σ is proportional to $\frac{\omega}{\Delta}$ and that the scaling function f in this approximation is a semicircle. Figures 12(a) and 12(b) contain the numerical solution for the density of states ρ_l and its scaling form f, as obtained from the second-order perturbation theory supplemented by the self-consistent condition near U_{c2}. They demonstrate that the region where scaling holds is actually quite large.

In principle, Eq. (20) can be expanded to next order in Δ, but the coefficient depends on the scaling function and the high-energy part of the Green's function and cannot be calculated analytically. However, it can be determined numerically that, close to the critical point, $\Delta = k(U_{c2} - U)$ with $k = 0.23$. Recalling the definition of $\Delta = zD$ and that $\frac{m^*}{m} = z^{-1}$, this last result implies that within this approximation we find the same critical behavior for the divergence of the renormalized mass as in the work of Brinkman and Rice.[3] Notice that within second-order perturbation theory $\frac{\partial^2 \Sigma}{\partial \omega^2}$ is not divergent as one would expect on general grounds. This is due to the fact that in this approach the vertex U is not renormalized.

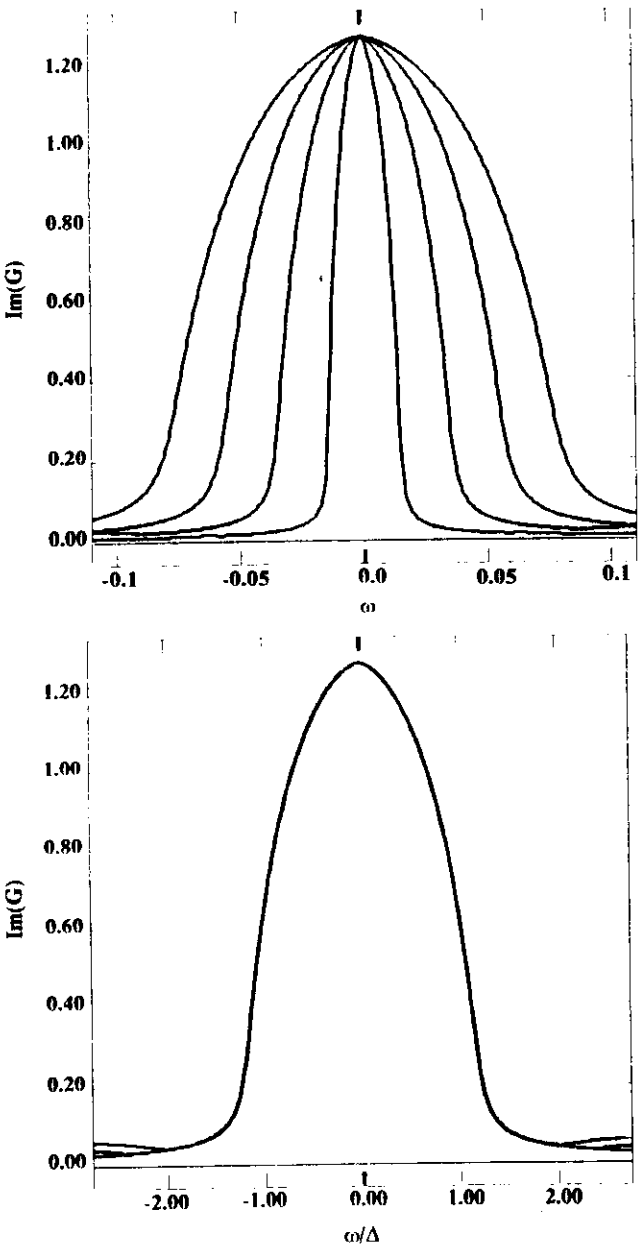

FIG. 12. (a) Low-frequency part of the density of states $\rho(\omega)$ as function of the frequency for values of the interaction $U = 3, 3.1, 3.2, 3.3$. (b) The four curves of (a) collapse to one universal form after rescaling: $f(\frac{\omega}{\Delta}) = t\rho_t(\omega)$, where $\Delta \propto U_c - U$.

V. THE BREAKDOWN OF THE INSULATING SOLUTION

In this section we study how the insulating solution disappears as we reduce the value of U. Our calculations determined that there indeed exists a new boundary $U_{c1}(T) < U_{c2}(T), U_{c1}(T = 0) \approx 2.6D$ associated with the breakdown of the insulating solution.[22]

To understand the destruction of the insulating state, we again proceed to parametrize the Green's function.

$$G_0(\tau) = \alpha[\theta(\tau) - 1/2] + G_0^{\rm inc}(\tau), \tag{23}$$

the first term with $\theta(\tau)$ being the step function, represents an insulating solution at the atomic limit (t=0). $G_0^{\rm inc}$ is the "incoherent part" of the insulating solution, which decays to zero as $\tau \to \infty$ at zero temperature. Physically, this decomposition is motivated by viewing the self-consistent equations as describing a Kondo spin in an insulator. The spin operator S has a low-energy part which is responsible for a Curie type of local spin susceptibility and a high-frequency part. We write $S = \sqrt{\alpha} S_{\rm low} + S_{\rm high}$, where α is a quantity similar to the quasiparticle weight, describing the weight of a pure free spin in an interacting system, the impurity plus the insulating host. In frequency space, $G_0^{\rm inc}$ is only responsible for the details of the shape of the Hubbard bands which are high-frequency features. The step-function part gives rise to a divergency in $G_0(i\omega_n) \sim 1/i\omega_n$ and is solely responsible for the existence of a gap. In the atomic limit, α approaches unity, while on the contrary, the vanishing of α signals the complete screening (or Kondo quenching) of the spin and the destruction of the insulating phase.

Using the parametrized form of G_0, we can relate α to the density of states $\rho(\epsilon)$ of the local Green's function. At half filling, because of the particle-hole symmetry,

$$G = 2i\omega_n \int_0^\infty \frac{\rho(\epsilon) d\epsilon}{(i\omega_n)^2 - \epsilon^2}. \tag{24}$$

Therefore, using (3) and comparing linear terms in $i\omega$,

$$\alpha^{-1} = 1 + 2t^2 \int_0^\infty \frac{\rho(\epsilon) d\epsilon}{\epsilon^2}. \tag{25}$$

If the Mott-Hubbard gap collapses, i.e., $\rho(\epsilon)$ becomes finite at $\epsilon \to 0$, α^{-1} diverges. Alternatively, a finite α at the transition indicates a finite Mott-Hubbard gap. Within the second-order perturbation scheme, we can obtain a closed equation for α. Inserting the parametrized G_0 into the self-energy expression we obtain

$$\Sigma(\tau) = \alpha^3 \left(\frac{U}{2}\right)^2 [\theta(\tau) - 1/2] + \Sigma_{\rm inc}, \tag{26}$$

which determines the low-frequency behavior of the local Green's function:

$$G = \frac{2}{\{i\omega_n + \Sigma(G_0) + i\mathrm{sgn}(\omega_n)\sqrt{D^2 + [\omega_n + i\Sigma(G_0)]^2}\}}. \tag{27}$$

Considering the most singular terms in the self-consistency condition in Eqs. (2) and (3), for small ω we have

$$G_0^{-1} = i\omega_n + \frac{D^2}{4\Sigma}, \tag{28}$$

and therefore,

$$\alpha = \left(1 + \frac{D^2}{U^2\alpha^3}\right)^{-1}. \tag{29}$$

There are two solutions for α^* for $U > U_{c1}$. The one with a smaller α^* is always unstable and unphysical since it is not connected continuously to $\alpha = 1$ as U tends to infinity. At the transition U_{c1}, the unstable fixed point collides with the stable one, and the fixed-point solution disappears. $U_{c1} = 3\sqrt{3}/2D \approx 2.6D$ which is the same as the result numerically obtained. Since α is finite at the transition, the Mott-Hubbard gap is finite. Across the critical line $U_{c1}(T)$ there is a first-order jump in the dielectric constant. There are, however, soft fluctuations associated with fluctuations in α . An important issue left open is whether α diverges as $U \to U_{c1}$ in the full solution. As was previously noted in Sec. II, we observed using QMC that in the exact finite-temperature solution the U_{c1} vs T line is shifted to lower values of U, indicating a further reduction of the minimum gap. We are not able to determine whether the gap collapses to zero as in Hubbard's original scheme ($\alpha \propto U - U_{c1}$), or whether it remines finite until it disappears, as described by the second-order perturbation scheme.

VI. SUSCEPTIBILITIES AND THE MOTT-HUBBARD TRANSITION

In what follows we are going to present a combination of theoretical arguments and numerical results, in order to discuss the behavior of the susceptibilities in the vicinity of the transition. Unfortunately, we cannot take further advantage of the perturbative approach. The vanishing of higher-order corrections in the self-energy in the atomic limit does not necessarily imply that this will be true also for the calculation of other quantities. Therefore, all the numerical results in this section were obtained with the QMC method. Although the present computational power does not allow a detailed quantitative analysis of higher correlation functions at very low temperatures, our results are sufficient to give support to the theoretical discussion.

Much theoretical insight about the behavior of the spin and charge susceptibilities can be gained from the fact that the impurity model describing the Hubbard model is an Anderson impurity model.

In a previous work we have already discussed the fact that, when the Mott point is approached, magnetic order of the local spin sets in.[13] This is observed from the plots of the imaginary-time spin-spin correlation function which exhibit a divergence in $\chi_L^s = \int_0^\beta \langle m_z(\tau)m_z(0)\rangle d\tau$, shown in Fig. 13.

In principle χ_L^s can be determined in NMR experiments. However, it is the $q = 0$ susceptibility that is easily accessible to experimental probes. The $q = 0$ quantities differ from the local ones because of the polarization of the Weiss field due to the external perturbation. We will illustrate how this effect, which is at the heart of Fermi liquid theory, modifies the low-energy responses near U_{c2}.

In the presence of a small chemical potential away from the particle-hole symmetric value and a small magnetic field, the mean-field equations are

$$G_{0\sigma}^{-1} = i\omega_n + \mu + \sigma h - t^2 G_\sigma. \tag{30}$$

To proceed, we extend the simplified form of the parametrization discussed in Sec. IV to account for the magnetic properties. The high-frequency part of the Green's function is polarized like a local moment which can be described as a superposition of Hartree-Fock solutions. It has been demonstrated that as $U \sim U_c$ the upper and lower Hubbard bands are well developed, so that for low frequencies and fields, a good approximation for G_σ is

$$G_\sigma = \frac{n_\sigma}{[i\omega_n - \frac{U}{2}]} + \frac{n_{-\sigma}}{(i\omega_n + \frac{U}{2})} + \frac{2}{D}\frac{\Delta}{i\omega_n + \Delta(\mathrm{sgn}\omega_n)}. \tag{31}$$

Inserting (31) in (30), we have for small frequencies,

$$G_{0\sigma}^{-1} = i\omega_n + \mu + h\sigma + 2\frac{t^2 m_\sigma}{U} \tag{32}$$

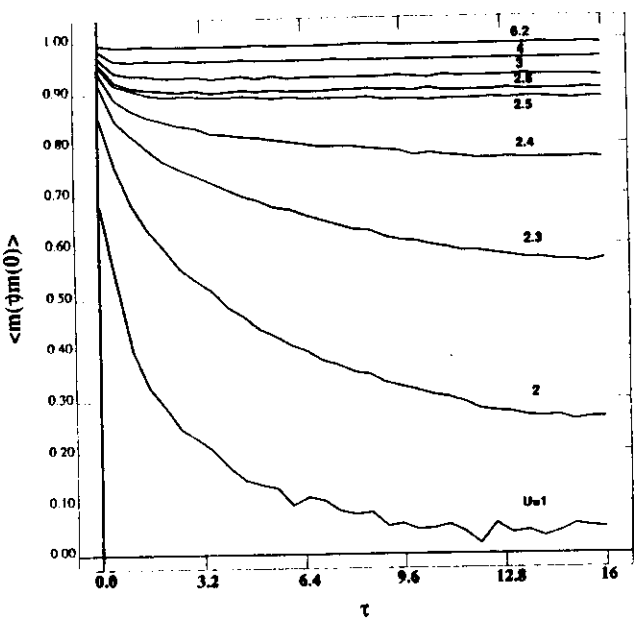

FIG. 13. Moment-moment correlation function as a function of imaginary time at $\beta = 32$. (See Ref. 28.)

where $n_\sigma = n + \frac{m_\sigma}{2}$. Equation (32) describes an impurity problem in the presence of an external field $h_{\rm eff} = h - 2\frac{t^2}{U}m_\sigma$. We can compute the magnetization from the theory of the Anderson impurity model in an effective field $h_{\rm eff}$. We know that $m = \chi_0 h_{\rm eff}$ with $\chi_0 \sim \frac{1}{\alpha T_k}$, where T_k is the effective Kondo energy of the problem, which in our case corresponds to Δ, and α is a numerical coefficient of order unity. Solving for m we find

$$\chi_s = \left[\frac{dm}{dh}\right]_{h=0} = \frac{1}{[\chi_0^{-1} + 2\frac{t^2}{U}]} = \frac{1}{\alpha\Delta + J_0} \tag{33}$$

where we have defined the magnetic exchange energy $J_0 = 2\frac{t^2}{U}(= \frac{D^2}{\alpha U})$.

The physical interpretation of this equation is transparent: the exchange arises from high-energy processes which are largely unaffected by the Mott transition. As a result the susceptibility varies continuously, as U passes through U_c. Remarkably, Eq. (33) was also obtained in the large-N limit.[23] These findings are consistent with the QMC results of Fig. 14. For smaller U, an initial fast increase in χ_s is observed as Δ rapidly decreases. As the critical value of U is approached we see the divergency being cut off by the finite magnetic exchange J_0.

Similar considerations apply to the charge susceptibility. Applying a chemical potential does not cause a change (to order δn) in the distribution of integrated spectral weight between the upper and lower Hubbard bands. This can be readily understood by extending the observation of Ref. 12 that the high-energy features are correctly reproduced by an expansion around the atomic limit. In this limit a small particle-hole asymmetry shifts the energies of the atomic levels but does not transfer spectral weight. The change in the low-energy part of the Green's function is easily estimated using Fermi liquid theorems. The change in $G(0)$ as a result of a change in chemical potential is given by the phase shift, which in turn is given by the shift of the location of the center of the resonance. Its width does not change to order Δ because of particle-hole symmetry. Assuming that at low frequencies the result of applying μ is to shift the center of the resonance by ϵ_f:

$$G(i\omega_n) \simeq \frac{\Delta}{(i\omega_r + \epsilon_f + i\Delta{\rm sgn}\omega_n)} \tag{34}$$

with $\delta n \simeq \frac{\epsilon_f}{\pi\Delta}$. We find $\delta G(0) = \frac{\delta n}{\Delta}$ and, therefore, from Eq. (30), the effective chemical potential seen in the impurity model is $\delta\mu_{\rm eff} = \delta\mu - \frac{t^2}{\Delta}\delta n$. The response of the impurity to this shift in the chemical potential is $\delta n = \chi_{\rm imp}\delta\mu_{\rm eff}$, with $\chi_{\rm imp} \simeq \frac{1}{U}$ the charge susceptibility of the impurity. Combining these equations we obtain:

$$\frac{\delta n}{\delta\mu} = \frac{\chi_c^0}{\left(1 + \frac{\chi_c^0 t^2}{\Delta}\right)} \simeq \Delta, \tag{35}$$

that is, the charge susceptibility vanishes as $(U_c - U)$ as we approach the Mott transition. These results are also consistent with the numerical simulations. Figure 15 shows the slope of the μ vs n curves going to zero as U approaches U_c. On the other hand, the moment $\langle(n_\uparrow - n_\downarrow)^2\rangle$, a quantity closely related to the double occupancy, does not saturate as the transition is crossed, as can be seen in Fig. 16. This is consistent with the *local* charge susceptibility being finite. In fact, the *impurity* charge compressibility equals minus the kinetic energy by virtue of the mean-field equations.

We argued before that the local spin susceptibility diverges at the Mott transition as $\frac{1}{\Delta}$ while the $q = 0$ spin susceptibility stays finite at the transition. This and an independent estimate of the exchange constant J_0 can be obtained by approaching the transition from the insulat-

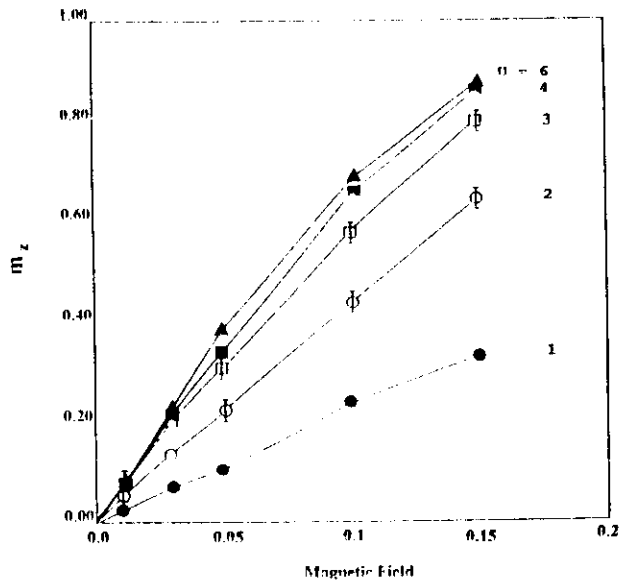

FIG. 14. Local magnetization m_z as function of an external magnetic field, for different values of the interaction U.

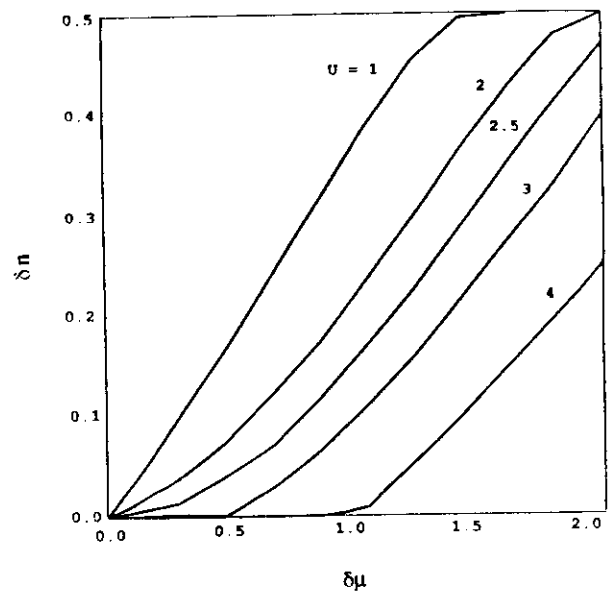

FIG. 15. Difference in the occupation number δn from the half-filled case as a function of the chemical potential $\delta\mu = \mu - U/2$, for different values of the interaction U.

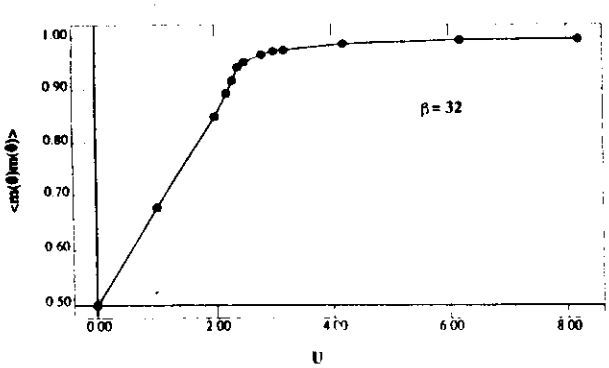

FIG. 16. Local magnetic-moment formation $\langle m_z^2 \rangle$ as a function of interaction U for inverse temperature $\beta = 32$. The double occupancy $\langle D \rangle$ can be simply obtained from $\langle m_z^2 \rangle = 1 - 2\langle D \rangle$. (See Ref. 28.)

ing side and by analyzing the fully frustrated model.

For large U, the fully frustrated model in Eq. (4) reduces at half filling to

$$H_J = \sum_{ij} J_{ij} S_i \cdot S_j, \tag{36}$$

where J_{ij} are independent random variables with an exponential distribution $P\{J\} = \frac{\Theta(J)}{\sqrt{J}} \exp - (JN/J_0)$, with $\theta(x) = 1$ for $x > 0$ and $\theta(x) = 0$ for $x < 0$.

An important observation is that $\bar{J}_{ij} = \frac{J}{N}$ while the variance $\bar{J}_{ij}^2 - \bar{J}_{ij}^2 = \frac{J^2}{N^2}$ so the randomness is irrelevant in the thermodynamical limit. The solution of Hamiltonian (36) with $J_{ij} = \frac{J}{N}$ is elementary.

We exhibit the solution to confirm and interpret the finite susceptibility in the insulating phase. The eigenstates of Eq. (36) are labeled by the total spin $\epsilon_s = \frac{J_0}{N}[S(S+1)]$. For simplicity we will take N to be even, $N \equiv 2N_0$. For a given value of the spin the degeneracy of a state with a given value of total spin S and projection S_Z is: $d_S = \binom{2N_0}{N_0 - S} - \binom{2N_0}{N_0 - S - 1}$. The partition function in the presence of a uniform field reduces to:

$$Z = \sum_{S=0}^{N_0} d_S e^{-\beta \frac{J_0}{2N_0} S(S+1)} \frac{\sinh[\beta h(S + \frac{1}{2})]}{\sinh(\frac{\beta h}{2})}. \tag{37}$$

In the thermodynamical limit $N_0 \to \infty$ it is convenient to introduce the variable $x = S/N_0$ and Eq. (37) reduces to

$$Z = N_0 \left\{ \int_0^1 dx e^{N_0 g(x)} e^{-\frac{\beta J_0 N_0 x^2}{4}} \times \left[\frac{e^{h\beta N_0 x} - e^{-h\beta N_0 x}}{2\sinh(\frac{h\beta}{2})} \right] + O\left(\frac{1}{N_0}\right) \right\} \tag{38}$$

with $g(x) \equiv \ln \frac{4}{(1+x)(1-x)} + x \ln[\frac{1-x}{1+x}]$ being the density of states. This system is peculiar in that the number of states decreases as the energy (or the spin) increases. $g(x) = 2\ln 2 - x^2$ as $x \to 0$, and therefore it has negative temperature. Equation (38) is easily evaluated when N_0 is large, and we obtain the free energy per particle

$$\frac{F(h,\beta)}{N} = -\frac{h^2\beta}{(8 + 2\beta J_0)} - \frac{1}{\beta}\ln 2, \tag{39}$$

and the susceptibility

$$\chi^s(q=0) = -\frac{\partial^2 f}{\partial h^2} = \frac{1}{(4T + J_0)}, \tag{40}$$

which displays the Curie law for $T \gg J_0$ but saturates at the magnetic energy J_0 at low temperatures, in complete agreement with the discussion of the paramagnetic phase. From the free energy we can extract the entropy and the energy $-E = \frac{\partial \ln Z}{\partial \beta}$ and $S = \frac{E-F}{T}$. Notice that when $h = 0, E = 0$ and $S = 2N_0 \ln 2$. This is the result of the large degeneracy of the singlet sector. In fact the number of states per particle in the singlet sector can be estimated directly from Eq. (39).

The prediction that χ^s remains finite as $U \to U_{c2}$ is physically sensible and probably persists in finite dimensions. It reflects the fact that the magnetic energy is finite when $d \to \infty$. The same is true in the limit of large N of the model studied in Ref. 24 in any dimension, provided we identify the Mott transition with the metal–charge-transfer-insulator transition. This physics is missed by the Gutzwiller approximation, which ignores the high-energy processes and thus the magnetic exchange completely. The divergence of γ (cf. Sec. III) as $U \to U_c$ is consistent with the fact that the entropy is ln2 in the insulator. In the metallic phases $S(T) = \int_0^T \frac{C_v(T')}{T'} dT'$. Since this quantity vanishes as $T \to 0$ in the insulating phase $\frac{C_v(T)}{T}$ diverges at the transition. This is the result of a large spin ground-state degeneracy. It is rooted in the fact that since $J_{ij} \sim \frac{1}{d}$ one needs long-range order to gain finite magnetic energy. This is clearly unrealistic and will not persist in any finite dimension. In fact, in the large-N limit in finite dimensions the specific heat remains finite when the metal-insulator transition drives the system into a resonating-valence-bond state.[25] It would be interesting to construct a loop expansion around the $d = \infty$ solution to remedy this problem.

We also demonstrated that for $U < U_{c2}$, the one-particle Green's function of the model captures some aspects of the Brinkman-Rice scenario. In particular, the mass renormalization diverges as $(U_{c2} - U)^{-1}$.[13] At the same time the solution of the Hubbard model in infinite dimension also allowed us to perform calculations of physical quantities at finite temperatures and eliminate some of the shortcomings of the Brinkman-Rice description of the Mott transition. In the actual solution, the number of doubly occupied sites is finite and changes smoothly at the metal-insulator transition[15,13] resulting in a finite exchange constant which gives rise to a finite susceptibility. We also observed that the single-particle gap opens discontinuously at U_{c2}, which is different from the predictions of the slave-boson method,[23] but is not inconsistent with the experimental observations of Fujimori *et al.*[26]

VII. COMPARISON WITH EXPERIMENTS

A theory of the Mott transition would be incomplete without a comparison to some of the existing experiments on the subject. Our goal here is to assess to what extent the Hubbard model in the limit of large dimensions capture the main trends of transition-metal oxides near the Mott transition, rather than to obtain the best possible fit to the experimental data.

We first focus on the beautiful set of experiments by the group of Tokura *et al.*, where the system $La_{1-x}Sr_xTiO_3$ is studied as a function of doping x.[19] They measured the specific heat coefficient γ as a function of x. Since the photoemission study shows that the $x = 0$ point is close to the Mott transition,[26] we picked $U = 3.2D$ and performed quantum Monte Carlo simulation to calculate γ vs doping. The results are shown in Fig. 17, together with the experimental data. The agreement is quite good.

We finally turn to the V_2O_3 system. This system was studied extensively before, and has been studied again most recently by Carter *et al.*[18] We have compared the experimental phase diagram with the one obtained for the two-sublattice fully frustrated model. On a qualitative level we find that the overall agreement is remarkably good, especially regarding the features of the three phase boundaries, antiferromagnetic insulator to paramagnetic metal, paramagnetic metal to paramagnetic insulator, paramagnetic insulator to antiferromagnetic insulator, and the crossover regime. Interestingly, we also found a small region of a metallic antiferromagnetic state similar to the experimental observation of Ref. 18. Unfortunately, it occurs at a very low temperature and the determination of the phase boundary is outside the applicability of the QMC method. Nevertheless the existence of this phase can be seen by a simple Hartree-Fock calculation in the frustrated case.

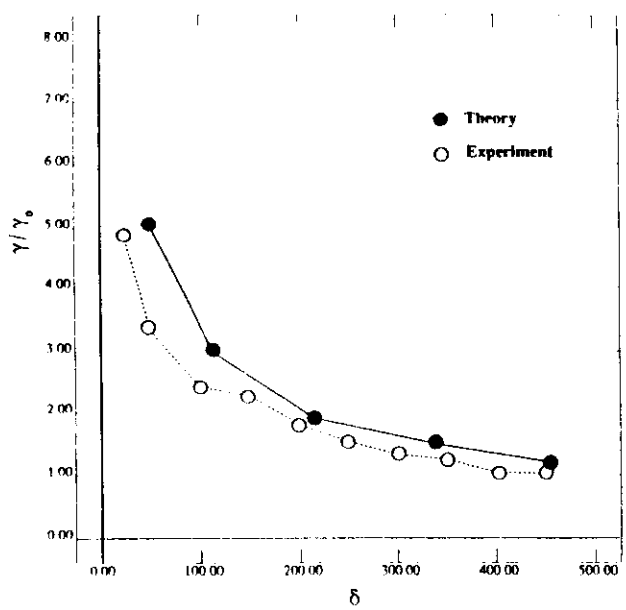

FIG. 17. Comparison to experimental observation of the linear coefficient of the specific heat γ as a function of doping for an inverse temperature of $\beta = 32$. Experimental results from Ref. 19. Quantities normalized to the full (or zero) filling value.

It is also notable that the temperature scales are consistent if an energy of $D = 1$ eV is considered. The comparison on the abscissa is less transparent. In this case, we have identified increasing pressure as increasing hopping constant t or decreasing interaction U.

VIII. CONCLUSION

The solution of the Hubbard model in the limit of large dimensions has provided a limit where various early ideas can be put in perspective.

One issue is whether a metal-insulator transition can take place in the absence of magnetic order. The phase diagram presented in Figs. 10 and 11 answers this question in the affirmative for a frustrated lattice. The phase diagram has the same topology and even the same scale as the experimentally observed phase diagram of V_2O_3.

There is a region enclosed by two lines $U_{c1}(T)$ and $U_{c2}(T)$, where both the metallic and the insulating solutions are allowed. Within this region, there is a first-order boundary where the two very different solutions cross in free energy, and several quantities experience a jump: the specific heat, the susceptibility, the number of doubly occupied sites, etc. The first-order line has a negative slope, indicating that the paramagnetic insulating phase has a higher entropy than the metallic phase. The line ends in an interesting second-order critical point, above which there is a smooth crossover between a metallic and an insulating regime. In the frustrated lattice, in addition, at low temperatures there is a first-order line between an antiferromagnetic metal and an antiferromagnetic insulating phase. We therefore conclude that the Hubbard model in large dimensions at half filling on a frustrated lattice can account for the basic experimentally observed features of the V_2O_3 system, vindicating Mott's point of view.

On nonfrustrated, bipartite lattices, however, we find that the Néel temperature is much higher than the metal-insulator transition temperature, making the transition between small and large U continuous. In this case the physics can be understood in terms of the magnetic long-range order and a smooth crossover within the broken-symmetry phase. The Mott transition is irrelevant, vindicating Slater's point of view.

Within the second-order perturbation scheme we establish that there is a metallic solution with a collapsing energy scale at U_{c2}, realizing the Brinkman-Rice scenario. We were unable to prove that this solution is stable down to U_{c2} because the energy differences between the metallic and insulating solutions are very small. However, assuming the stability of the solution we were able to calculate the critical behavior of various physical quantities and make contact with the recent experiments of Ref. 19. We conclude that the Hubbard model in large dimensions, therefore, supports the Brinkman-Rice scenario for the destruction of the metal and eliminates many of its shortcomings.

A natural scenario for the destruction of the insulating solution would be a continuous narrowing of the gap of the insulator. This would have been a realization of the original Hubbard scenario for the metal-insulator transition driven by the closing of the upper and lower Hubbard bands. In this case, U_{c1} would have corresponded to the value of the interaction where the gap in the one-particle spectra vanishes, or equivalently where the divergence of the dielectric constant is observed. This does not occur, at least within the second-order approximation to the impurity self-energy.

The experimentally observed phase diagrams of transition-metal oxides display incommensurate metallic magnetism. This can in principle be studied by extending the mean-field theory to account for incommensurate phases, as done by Freericks for the Falicov-Kimball model.[27] For this calculation to be meaningful, however, one should include the details of a realistic band structure of the transition-metal oxide, which is beyond the scope of our work.

An important open question is what happens to the transition at finite dimensions? We expect that the Mott transition and the metal–charge-transfer-insulator transition are in the same universality class. The large-N expansion results of Ref. 24 indicate that, for $N = 2$, U_{c1} and U_{c2} coincide and that the Mott transition is second order with continuous disappearance of the Kondo resonance and a gradual closing of the Mott gap. Similar results were obtained with the slave-boson approach to the Hubbard model. Whether the large-N expansion is missing crucial $1/N$ terms which would split the two transitions, or whether the $1/d$ corrections would bring the two transitions to one, remains an interesting open problem.

Note added in proof. Recently, two zero-temperature algorithms based on exact diagonalization were developed.[29,30] We have confirmed that U_{c1} is strictly less than U_{c2} and shown that the MIT at $T = 0$ takes place at U_{c2}.[31]

ACKNOWLEDGMENT

We want to thank D. Fisher and A. Georges for an illuminating discussion that motivated part of this work. We also had very useful conversations with V. Dobrosalevic, F. Gebhard, and Q. Si. The numerical part of this work was performed on a Cray Y/MP supercomputer of the NCSA in the University of Illinois at Urbana-Champaign. This work was supported by the NSF under Grant No. DMR-92-24000.

[4] N. F. Mott, Philos. Mag. **6**, 287 (1961).
[2] J. Hubbard, Proc. R. Soc. (London) **A281**, 401 (1964).
[3] W. F. Brinkman and T. M. Rice, Phys. Rev. B **2**, 4302 (1970).
[4] J. C. Slater, Phys. Rev. **82**, 538 (1951).
[5] W. Metzner and D. Vollhardt, Phys. Rev. Lett. **62**, 324 (1989).
[6] U. Brandt and C. Mielsch, Z. Phys. **75**, 365 (1989); **79**, 295 (1990); **82**, 37 (1991).
[7] V. Janis, Z. Phys. B **83**, 227 (1991).
[8] E. Müller-Hartmann, Z. Phys. B **74**, 507 (1989); Z. Phys. B **76**, 211 (1989).
[9] A. Georges and G. Kotliar, Phys. Rev. B **45**, 6479 (1992).
[10] V. Janis and D. Vollhardt, Int. J. Mod. Phys. B **6**, 731 (1992).
[11] A. Georges, G. Kotliar, and Q. Si, in *Proceedings of the Trieste Meeting on Strongly Correlated Electron Systems* [Int. J. Mod. Phys. B **6**, 705 (1992)].
[12] M. J. Rozenberg, X. Y. Zhang, and G. Kotliar, Phys. Rev. Lett. **69**, 1236 (1992).
[13] X. Y. Zhang, M. J. Rozenberg, and G. Kotliar, Phys. Rev. Lett. **70**, 1666 (1993).
[14] M. Jarrell, Phys. Rev. Lett. **69**, 168 (1992); Th. Pruschke, D. L. Cox, and M. Jarrell, Eur. Phys. Lett. **21**, 5 (1993); Phys. Rev. B. **47**, 3553 (1993).
[15] A. Georges and W. Krauth, Phys. Rev. Lett. **69**, 1240 (1992).
[16] A. Georges and W. Krauth Phys. Rev. B **48**, 7167 (1993).
[17] V. Janis, M. Ulmke, and D. Vollhardt (unpublished).
[18] S. A. Carter, T. F. Rosenbaum, J. M. Honig, and J. Spalek, Phys. Rev. Lett. **67**, 3440 (1992).
[19] Y. Tokura, Y. Taguchi, Y. Okada, Y. Fujishima, T. Arima, K. Kumagai, and Y. Iye, Phys. Rev. Lett. **70**, 2126 (1993).
[20] A. Georges and S. Sachdev (unpublished).
[21] K. Yamada, Prog. Theor. Phys. **53**, 970 (1975); K. Yosida and K. Yamada, *ibid.* **53**, 1286 (1975).
[22] This possibility was suggested to us by D. Fisher as a way of reconciling the numerical results of our group and those of the ENS group.
[23] G. Kotliar, Int. J. Mod. Phys. B **1**, 711 (1988).
[24] C. Castellani, G. Kotliar, R. Raimondi, M. Grilli, Z. Wang, and M. Rozenberg, Phys. Rev. Lett. **68**, 2009 (1992).
[25] M. Grilli and G. Kotliar, Phys. Rev. Lett. **64**, 1170 (1990).
[26] A. Fujimori, I. Hase, H. Namatame, Y. Fujishima, Y. Tokura, H. Eisaki, S. Uchida, K. Takegahara, and F. M. F. de Groot, Phys. Rev. Lett. **69**, 1796 (1992).
[27] J. Freericks (unpublished).
[28] Figures 13 and 16 contain small corrections to the corresponding figures of Ref. 13.
[29] Q. Si, M. J. Rozenberg, G. Kotliar, and A. Ruckenstein (unpublished).
[30] M. Caffarel and W. Krauth (unpublished).
[31] M. J. Rozenberg, G. Moeller, and G. Kotliar (unpublished).